

# Chapter 2

## Hydrogen Production Processes

Lúcia Bollini Braga, Márcio Evaristo da Silva, Túlio Stefani Colombaroli,  
Celso Eduardo Tuna, Fernando Henrique Mayworm de Araujo,  
Lucas Fachini Vane, Daniel Travieso Pedroso, and José Luz Silveira

### 2.1 Introduction

The main hydrogen production processes can be classified into electrolysis, photolysis, and thermolysis. Electrolytic hydrogen production processes involve the use of electric or thermal energy to trigger a chemical reaction for splitting water molecules into hydrogen and oxygen. The main examples of electrolytic processes are water electrolysis (conventional process) and thermolysis (steam electrolysis). Photolytic processes involve technologies that use the energy of light, and its main examples are the photobiological and photoelectrochemical systems. Hydrogen production through thermochemical processes essentially comprise the raw material, being either from fossil or renewable sources, heat and catalysts so as to trigger chemical reactions for transforming the raw material (for example, ethanol, natural gas, methanol, gasoline) into hydrogen. The main thermochemical hydrogen production processes are: biomass gasification and pyrolysis, steam reforming, partial oxidation, autothermal and oxidative reforming (Braga 2010; Silva 2010).

---

L.B. Braga • M.E. da Silva • T.S. Colombaroli • C.E. Tuna • F.H.M. de Araujo • L.F. Vane • D.T. Pedroso

Group of Optimization of Energy Systems—GOSE, College of Engineering of Guaratinguetá, Institute of Bioenergy Research—IPBEN, São Paulo State University—UNESP, Dr. Ariberto Pereira da Cunha Avenue, 333, Guaratinguetá 12516-410, SP, Brazil

J.L. Silveira (✉)

Group of Optimization of Energy Systems—GOSE, College of Engineering of Guaratinguetá, Institute of Bioenergy Research—IPBEN, São Paulo State University—UNESP, Dr. Ariberto Pereira da Cunha Avenue, 333, Pedregulho, Guaratinguetá 12516-410, São Paulo, Brazil

e-mail: [joseluz@feg.unesp.br](mailto:joseluz@feg.unesp.br)

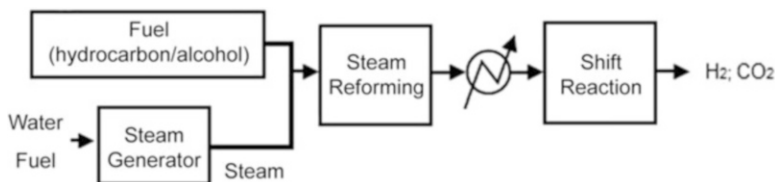


**Fig. 2.1** Steam reforming process flow chart (Adapted from Spath and Mann 2000)

## 2.2 Steam Reforming for Hydrogen Production

Steam reforming has been used as the main process for hydrogen production, which accounts for 50 % of the world's total production. The popularity of this process derives from its high conversion efficiency and cost-effectiveness in comparison with other processes (Chena et al. 2008). Figure 2.1 shows a simple reforming process flow chart.

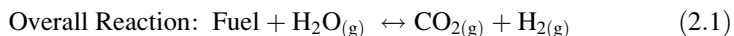
As illustrated in Fig. 2.1, this process occurs in two main steps, one that occurs at high temperatures (*steam reforming*), in which the fuel (hydrocarbon or alcohol) reacts with steam and is converted into a gaseous mixture of  $H_2$ ,  $CO$ ,  $CO_2$ , hydrocarbon or alcohol, and unreacted steam, and another one which occurs at lower temperatures in a *shift* reactor (water-gas shift reaction), where the  $CO$  present in the synthesis gas reacts with  $H_2O$  to produce additional  $CO_2$  and  $H_2$ .

Depending on the specifications of the fuel cell being used, an additional step of  $CO$  removal is necessary to purify the synthesis gases.

The main reactions involved in the steam reforming process are shown in Eqs. (2.1)–(2.3). Many chemical reactions can occur while the steam reforming reaction takes place simultaneously, and such reactions are presented in Eqs. (2.4)–(2.7) (Trane et al. 2012).

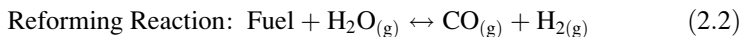
### 1. Overall Reforming Reaction

The overall reaction of fuel conversion into hydrogen by steam reforming is shown in Eq. (2.1).



### 2. Steam Reforming Reaction

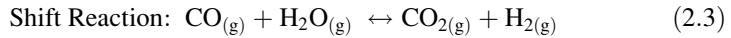
Equation (2.2) shows the steam reforming reaction which consists of an endothermic catalytic reaction of the fuel with steam, mainly producing carbon monoxide and hydrogen:



### 3. Water-Gas Shift Reaction

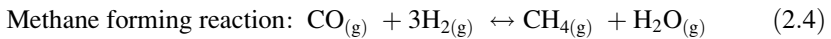
Equation (2.3) shows the catalytic water-gas shift reaction that produces additional hydrogen and eliminates part of the carbon monoxide, which is conducted through a catalytic reactor called as the *shift reactor*, i.e., the carbon monoxide reacts with steam so as to form carbon dioxide and hydrogen. This reaction is

carried out at lower temperatures, ranging from 200 to 300 °C (Casanovas et al. 2010).



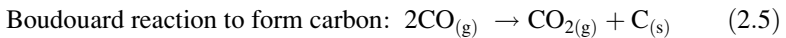
#### 4. Methane Formation Reaction

Equation (2.4) shows one of the reactions that can occur during the reforming process. The methane formation reaction is unwanted, since part of the produced hydrogen reacts with carbon monoxide, thus decreasing its composition in the final synthesis gas.



#### 5. Boudouard's Carbon Formation Reaction

One should consider, moreover, the possibility of producing carbon by decomposing carbon monoxide through the so-called Boudouard reaction, as shown in Eq. (2.5).



In order to illustrate the steam reforming processes, the pictures of two prototypes developed by the Group of Optimization of Energy Systems are shown in Figs. 2.2 and 2.3.

Figure 2.2 shows the prototype for the steam reforming of ethanol, which was funded by the P&D ANEEL Project of CEMIG (Companhia Energética de Minas Gerais). This equipment is powered by electricity, consisting of a steam generator, a steam reforming reactor, and a *shift reactor*.

Figure 2.3 shows a prototype for the steam reforming of biogas, which is also an electric prototype, consisting of a steam generator, a steam reforming reactor, and a shift reactor, all developed through the Research in Public Policies—FAPESP.

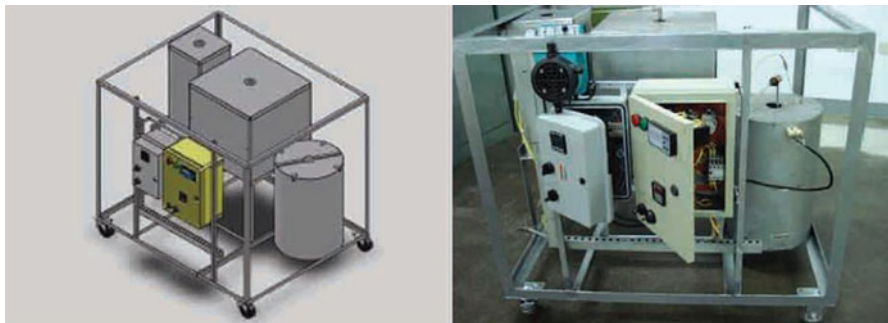


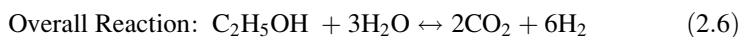
**Fig. 2.2** Prototypes for the steam reforming process of ethanol

**Fig. 2.3** Prototype for the steam reforming process of biogas

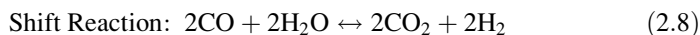
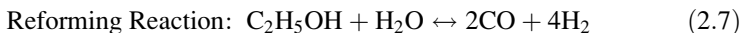


### ***2.2.1 Steam Reforming of Alcohols***

According to Silva (2005), a fairly feasible alternative is the production of hydrogen via the steam reforming of alcohols. In particular, the steam reforming of ethanol is quite interesting on account of the fact that Brazil is one of the major producers of sugarcane, being the leading producer and distributor of ethanol as fuel. The stoichiometry of the overall reforming process is presented by Eq. (2.6) (Silveira et al. 2009).

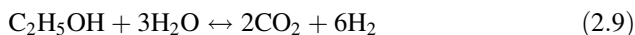


This equation is derived from the reforming and shift reactions, as indicated in Eqs. (2.7) and (2.8), respectively (Silveira et al. 2009).



The steam reforming reaction of ethanol occurs at temperatures between 400 and 700 °C (Saebea et al. 2011), and the shift reaction occurs at temperatures between 200 and 300 °C, as previously presented in Sect. 2.1.

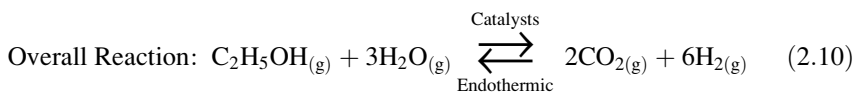
Among the methods of hydrogen production is the steam reforming of methane, which is a process that has been intensively studied. Another alternative which is quite feasible is the production of hydrogen via the steam reforming of alcohols. In particular, the steam reforming of ethanol is rather interesting, once again being due to the fact that Brazil is one of the major producers of sugarcane, and the leading producer and distributor of ethanol as fuel. Furthermore, the overall reaction of hydrogen production from ethanol corresponds to 6 mol of hydrogen formation per mole of ethanol consumed, according to the stoichiometry in Eq. (2.9).



This reaction, however, occurs in two steps: one at high temperatures (*steam reforming*), in which ethanol is converted into a gaseous mixture of  $\text{H}_2$ ,  $\text{CO}$ ,  $\text{CO}_2$ ,  $\text{CH}_4$ , and unreacted  $\text{H}_2\text{O}$ , and another at lower temperatures (water-gas shift reaction WGS), in which  $\text{CO}$  reacts with  $\text{H}_2\text{O}$  to form additional  $\text{CO}_2$  and  $\text{H}_2$ . Due to the shift reaction being limited by the equilibrium constant, the conversion of  $\text{CO}$  is incomplete and an additional step of  $\text{CO}$  removal is required to purify the synthesis gases. The steam reforming of ethanol technology involves a catalytic process that consists of an endothermic reaction between ethanol and steam. The chemical thermodynamic analysis of the steam reforming process of ethanol for obtaining hydrogen reveals that the process does not occur in a single step, and is linked to the following reactions:

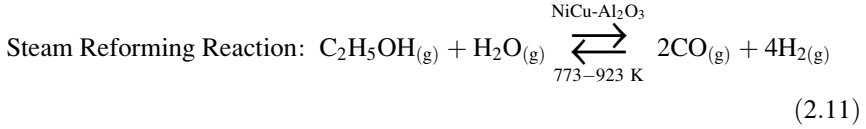
- *Overall Steam Reforming Reaction of Ethanol:*

The overall reaction of ethanol conversion into hydrogen produces 6 mol of hydrogen from 1 mol of ethanol through the steam reforming process, as shown in Eq. (2.10) using a steam/ethanol molar ratio of 3:



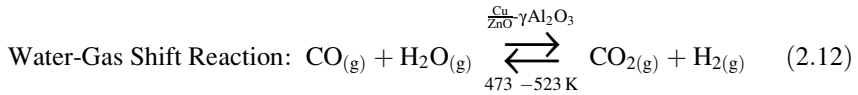
- *Steam Reforming Reaction:*

Equation (2.11) shows the steam reforming reaction which consists of an endothermic reaction of ethanol, mainly forming carbon monoxide and hydrogen through a steam reforming reactor with a catalytic bed at temperatures ranging between 973 and 773 K (external steam reforming: reformers) or through fuel cells, e.g., MCFC and SOFC, which are capable of performing internal steam reforming.



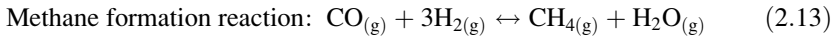
- *Water-Gas Shift Reaction:*

Equation (2.12) shows the water-gas shift reaction that is aimed at producing hydrogen and eliminating part of the carbon monoxide, which is accomplished through a catalytic reactor called as the shift reactor, i.e., carbon monoxide reacts with steam to form carbon dioxide and hydrogen. This reaction occurs at lower temperatures, ranging from 473 to 523 K, and on account of the water-gas shift reaction being limited by the equilibrium constant, the carbon monoxide conversion is incomplete, thus requiring an additional removal step in the case of feeding a PEM fuel cell whose operation requires minimal amounts of carbon monoxide.



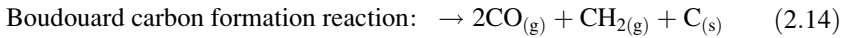
- *Methane Formation Reaction:*

Many chemical reactions can occur while the steam reforming reaction of ethanol is taking place simultaneously. Equation (2.13) shows the most significant reaction, i.e., the methane formation reaction ( $\text{CH}_4$ ) from ( $\text{CO}$ ), which should be added to the steam reforming reaction.



- *Boudouard's Carbon Formation Reaction:*

One should consider, moreover, the possibility of forming carbon by decomposing carbon monoxide through the so-called Boudouard reaction, as shown in Eq. (2.14).



The equilibrium constants associated with the reactions represented by Eqs. (2.15)–(2.18) can be expressed as:

$$K_1 = \frac{y_{\text{CO}_2}^2 y_{\text{H}_2}^6}{y_{\text{EtOH}} y_{\text{H}_2\text{O}}^3} P^4 \quad (2.15)$$

$$K_2 = \frac{y_{\text{CO}}^2 y_{\text{H}_2}^4}{y_{\text{EtOH}}^2 y_{\text{H}_2\text{O}}} P^4 \quad (2.16)$$

$$K_3 = \frac{y_{\text{CO}_2} y_{\text{H}_2}}{y_{\text{CO}} y_{\text{H}_2\text{O}}} \quad (2.17)$$

$$K_4 = \frac{y_{\text{CH}_4} y_{\text{H}_2\text{O}}}{y_{\text{CO}} y_{\text{H}_2}^3} P^{-2} \quad (2.18)$$

In which:  $P$  is the total pressure and  $y_i$  are the molar fractions of the gaseous components, which can be expressed by Eq. (2.19).

$$y_i = \frac{n_i}{n_{\text{TOT}}} \quad (2.19)$$

The equilibrium constants of reactions are related to the Gibbs free energies of the molecules involved in the equilibrium, which can be determined once the absolute temperature is specified. Once the temperature is determined, it is possible to calculate the equilibrium constants from thermodynamic data, as described by Maggio et al. (1998).

## 2.2.2 Physicochemical Analysis

### 2.2.2.1 Temperature Influence

The *Gibbs free energy* dependence on temperature can be expressed in several different ways, depending on the problem scale, as shown in Eqs. (2.20) and (2.21) and in Fig. 2.4.

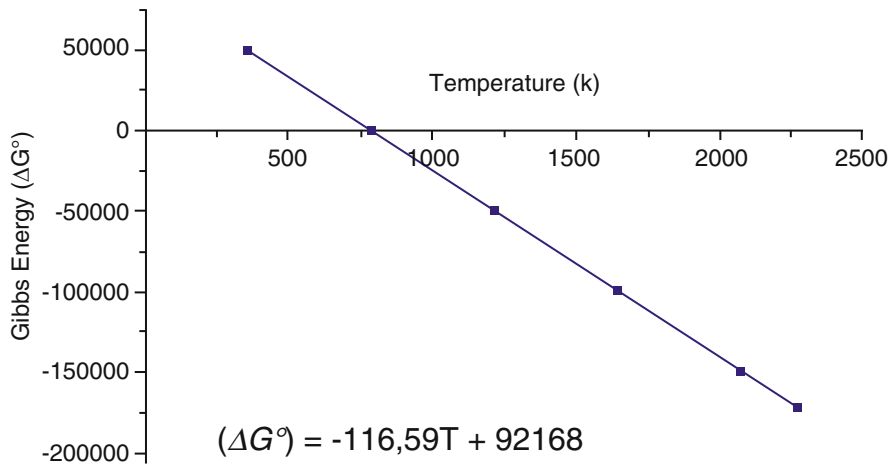


**Fig. 2.4** Gibbs free energy variation as a function of temperature

$$\Delta G^0 = \Delta H^0 - T \cdot S^0 \quad (2.20)$$

$$d\left(\frac{\Delta G^0}{T}\right) = \frac{-\Delta H^0}{T^2} \quad (2.21)$$

Figure 2.4 shows the Gibbs energy variation as a function of temperature for the steam reforming of ethanol.

The reforming reaction is endothermic,  $\Delta H^0$  is positive and the equilibrium constant increases as temperature does. Figure 2.4 shows the Gibbs free energy change ( $\Delta G^0$ ) as a function of temperature, in which it can be observed that it becomes null once it is close to 790 K, thus indicating that the reaction occurs at high temperatures. The straight line intersection with the horizontal axis presents a positive value, which indicates that the reaction is endothermic.

According to Le Chatelier's principle, increasing the temperature of the steam reforming reaction of ethanol will lead to a greater formation of products. Therefore, the overall reaction of the steam reforming of ethanol is favored by temperature increase, i.e., the chemical equilibrium of products is increased as temperature is raised.

### 2.2.2.2 Equilibrium Composition

The reaction's degree of advancement and Gibbs free energy decrease will continue until the system's Gibbs free energy reaches a minimum value, condition in which the reaction will be in equilibrium. The equilibrium composition as a function of temperature can be determined by setting the chemical equilibrium of the overall reaction, (Eq. (2.9)), as shown in Table 2.1.

By assuming an ideal behavior and disregarding the fugacity coefficients, equilibrium constant  $K$  equals  $K_p$  (equilibrium constant as a function of the partial pressure of each component). Once the molar fractions of each component in equilibrium are known, the equilibrium constant, (Eq. (2.9)), and the degree of advancement ( $\alpha$ ) of the overall steam reforming of ethanol reaction are determined, as shown in Table 2.2.

**Table 2.1** Chemical equilibrium of the overall steam reforming reaction

	C <sub>2</sub> H <sub>5</sub> OH +	3H <sub>2</sub> O	↔ 2CO <sub>2</sub>	6H <sub>2</sub>
<i>Start</i>				
N° mols $n_i$	$n$	$3n$	0	0
N° mols total $n_{TOT}^{(start)}$	$n_{TOT}^{(start)} = n + 3n = 4n$			
<i>At equilibrium</i>				
N° mols $n_i$	$n(1 - \alpha)$	$3n(1 - \alpha)$	$2n\alpha$	$6n\alpha$
N° mols total $n_{TOT}^{(equil.)}$	$n_{TOT}^{(equil.)} = 4n(1 + \alpha)$			
Molar fractions $y_i$	$y_{EtOH}$	$y_{H_2O}$	$y_{CO_2}$	$y_{H_2}$
	$\frac{1}{4}(1 - \alpha)/(1 + \alpha)$	$\frac{3}{4}(1 - \alpha)/(1 + \alpha)$	$\frac{1}{2}\alpha/(1 + \alpha)$	$3\frac{1}{2}\alpha/(1 + \alpha)$

\*(i) represent the overall reaction components



**Table 2.2** Equilibrium constant and degree of advancement

Equilibrium constant	$K$	$K = \frac{3^3 \cdot \alpha^8 \cdot P^4}{(1+\alpha)^4 \cdot (1-\alpha)^4} = \frac{27 \cdot \alpha^8}{(1-\alpha^2)^4} \cdot P^4$
Degree of advancement	$\alpha$	$\alpha = \frac{\sqrt[8]{K}}{\sqrt{\sqrt[4]{K} + \pm \sqrt[4]{27 \cdot P}}}$

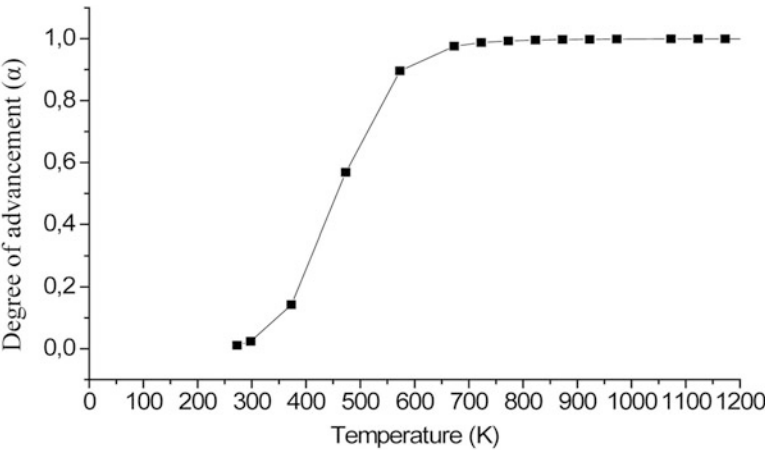


**Fig. 2.5** Degree of advancement of the overall steam reforming reaction of ethanol as a function of temperature

The values of equilibrium constant, degree of advancement, molar fractions of hydrogen and ethanol as a function of temperatures ranging from 273 to 1473 K and pressure of 0.101 MPa were calculated from the equations presented in Table 2.2. The degree of advancement as a function of temperature can be analyzed through Fig. 2.5.

It can be observed that the increase in temperature favors the advancement of the overall steam reforming reaction of ethanol, consequently the hydrogen production itself. The percentages of hydrogen and carbon dioxide produced as a function of temperature, and the percentages of hydrogen produced and remaining ethanol as a function of temperature, respectively, can be analyzed in Figs. 2.6 and 2.7.

It can be observed that, in Figs. 2.6 and 2.7, hydrogen production is favored by increased temperature, reaching a maximum value of production that is close to 600–650 K, then remaining constant from this temperature range.

2.2.2.3 Pressure Influence

According to Le Chatelier’s principle, an increase in the operating pressure of the overall steam reforming reaction of ethanol is going to lead to a shift in the equilibrium of the reaction in order to decrease the number of moles. That is, an

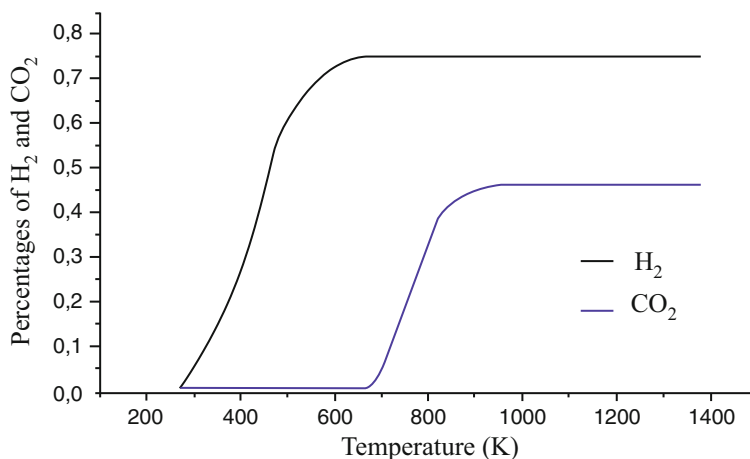


**Fig. 2.6** Percentages of hydrogen and carbon dioxide produced as a function of temperature

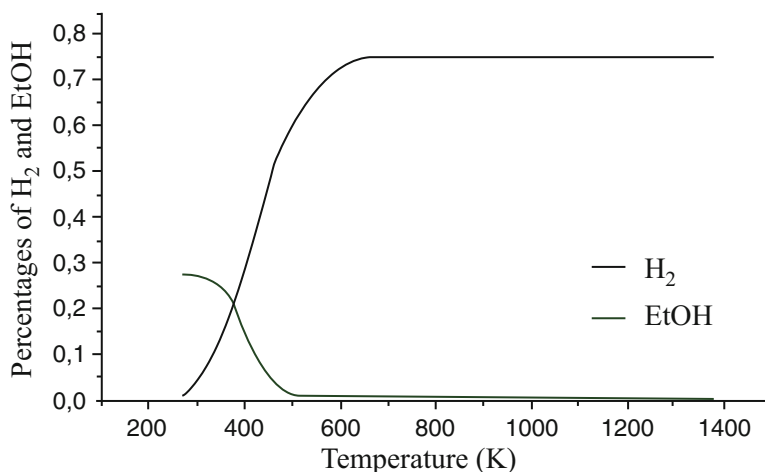


**Fig. 2.7** Hydrogen production and remaining ethanol percentage as a function of temperature

increase in pressure shifts the equilibrium towards the reactants. The analysis of equations in Table 2.2 shows that increased pressure causes a decrease in the degree of advancement of the overall steam reforming reaction of ethanol and, consequently, in hydrogen production.

Figure 2.8 shows this behavior of the degree of advancement of the overall steam reforming reaction of ethanol as a function of different pressures and temperatures.

It can be observed that, with the exception of this behavior in the temperature range of 573 K, the degree of advancement does not vary significantly as pressure does. Therefore, it can be concluded that pressure does not favor hydrogen production.

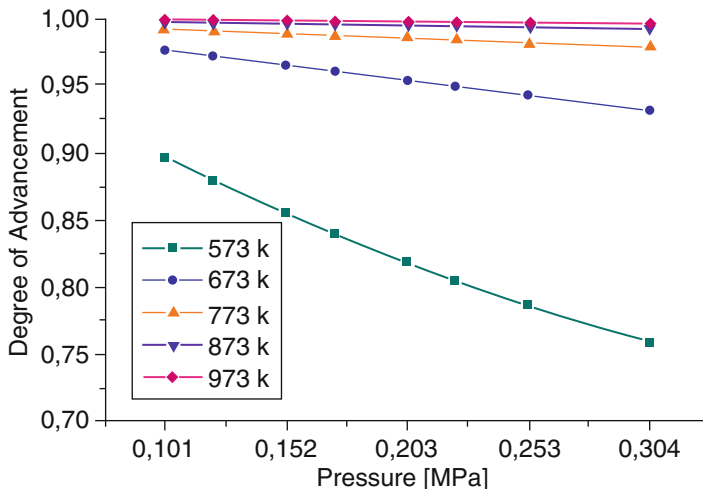


**Fig. 2.8** Degree of advancement as a function of pressure at different temperatures

### 2.2.3 Steam Reforming of Natural Gas and Biogas

The steam reforming process using natural gas accounts for 50 % of the world's hydrogen production. Natural gas has a similar origin to petroleum: it originated over millions of years through the decomposition of plants and animals, i.e., it is a nonrenewable fuel. Its composition shows some variations according to its origin and processing, being composed mainly of methane (about 90 %), ethane (from 5 to 8 %), propane, and traces of heavier hydrocarbons, moreover, it presents inert gases such as nitrogen, carbon dioxide, and helium (Krona et al. 2012).

Biogas can be a renewable alternative as raw material for conventional steam reforming. As natural gas, it is a mixture which is composed mainly of methane, and it results from an anaerobic fermentation of organic matter. In addition, if compared to natural gas, it offers the following benefits: it reduces methane emissions by the use of organic matter that would be released into the environment (methane is 21 times more harmful than carbon dioxide as regards the greenhouse effect) and it can be produced commercially on a large scale through the decomposition of organic matter from various sources (agricultural waste, tree-pruning waste, organic waste, industrial waste, sewage, animal waste, etc.) (Kothari et al. 2008). Depending on the biodigestion technology and the raw material being used, the composition of biogas varies between 45 and 75 % of  $\text{CH}_4$  and 25–55 % carbon dioxide, in addition to containing traces of hydrogen, sulfur, ammonia, and steam (Scholz et al. 2013).

Hydrogen production processes by the steam reforming of natural gas and biogas are based mainly on the steam reforming of methane, since it is the major constituent of both fuels. Reforming processes have contributed effectively to an increased

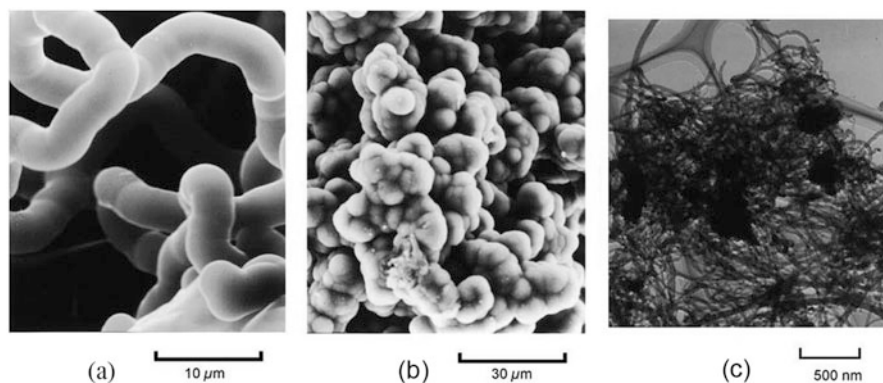


**Fig. 2.9** SEM (Scanning Electron Microscope) images of carbon deposition on Nickel cermets (Reproduced from Takeguchi et al. 2002)

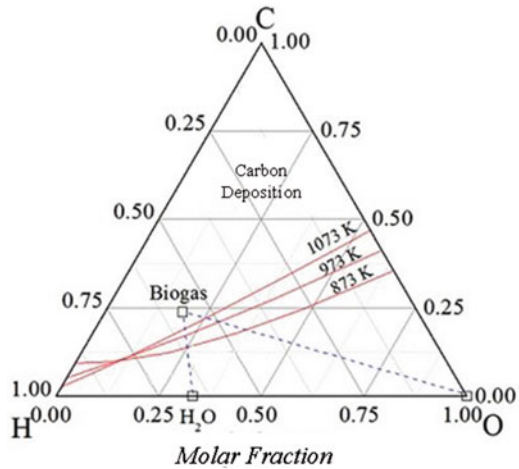
utilization of fuel cells because, through these processes, the possibilities of using fuel in these devices are increased, in addition to minimizing typical problems that arise from the use of such cells.

A major drawback found in different types of existing fuel cells is that the inputs used for feeding them should be homogeneous. Low-temperature fuel cells, such as polymer electrolyte membrane fuel cells, are only run on high-purity hydrogen; on the other hand, high-temperature cells can be run on more diverse compositions, where hydrocarbon-based fuels are mainly used because of their high hydrogen content. However, this often results in the formation of layers of solid carbon on the anode, which is a phenomenon known as carbon deposition. It drastically reduces the electrochemical performance of the fuel cell because it decreases the electrochemically active area, resulting in an increase in polarization strength and probably causing irreversible microstructural damages, such as metal dusting or catastrophic carburization, which leads to the disintegration of the metal, thus producing thin metallic dust and carbon (Kuhn and Kesler 2015). Figure 2.9 illustrates the carbon deposition on Nickel cermets,<sup>1</sup> being that (a) and (b) show a sample of Nickel cermet with yttrium stabilized on zirconia (Ni-YSZ) and (c) illustrates a nickel catalyst supported on zirconium II oxide ( $\text{ZrO}_2$ ).

In a study conducted by Wongchanapai et al. (2013), it was shown the influence of the addition of reforming agents, like oxygen and steam, on the performance of solid oxide fuel cells. In Fig. 2.9 it is noted the influence of temperature and composition on carbon deposition on the anode. The temperature lines in red are the deposition boundaries; each point belonging to this line is the limit composition so that there is no carbon formation in the solid oxide cell. Compositions that are above the aforementioned lines favor carbon deposition, and those below the lines

<sup>1</sup>Cermet: A composite material composed of ceramic (CER) and metallic (MET) materials.

**Fig. 2.10** Ternary diagram C-H-O with carbon deposition boundary in a solid oxide fuel cell (Reproduced from Wongchanapai et al. 2013)

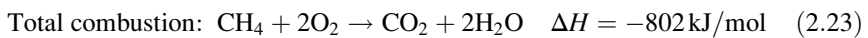
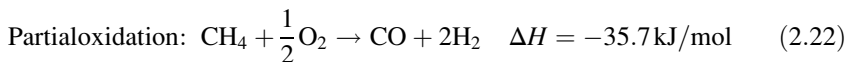


contribute to non-deposition. It is reasonable to expect that, once reforming agents are added ( $\text{H}_2\text{O}_{\text{steam}}$  and  $\text{O}_2$ ), the molar fraction will tend to be at the base of the ternary diagram (decreased concentration of C), i.e., for non-carbon deposition. Temperature also contributes to preventing carbon formation, i.e., the more it increases, the higher the deposition boundary will be (Fig. 2.10).

### 2.2.3.1 Partial Oxidation Reforming

- Partial oxidation:

Partial oxidation (Eq. (2.22)) is similar to the total combustion of methane (Eq. (2.23)), but it differs due to an insufficient amount of oxygen for complete combustion, thus producing only hydrogen and carbon monoxide as by-products.



The presence of  $\text{O}_2$  reduces carbon deposition at high temperatures, which increases the lifetime of the catalyst; however, the need for pure  $\text{O}_2$  pushes up the costs of the plant, as it requires a cryogenic air separation unit. On an industrial scale, the process of partial oxidation of methane is not fully established, mainly because there might be a power supply and reaction medium with  $\text{CH}_4$  and  $\text{O}_2$ , thus resulting in complete combustion and entailing risks of explosions (Vasconcelos 2006).

### 2.2.3.2 Dry or CO<sub>2</sub> Reforming

The CO<sub>2</sub> reforming of methane, also known as dry reforming (Eq. (2.24)), consists in an alternative route for synthesis gas production.

The high CO<sub>2</sub> content available on biogas offers a very interesting alternative to produce hydrogen from the reaction of CO<sub>2</sub> with methane, although the yield is lower if compared to that of the steam reforming reaction (Piroonlerkgul et al. 2008).



This is an endothermic process that produces a H<sub>2</sub>/CO ratio of 1, being suitable for the production of oxygenated compounds and high-purity carbon monoxide (Vasconcelos 2006).

### 2.2.3.3 Steam Reforming

The steam reforming of methane for hydrogen production achieves high conversion efficiency, and presents itself as a simple, low-cost technology. It is probably the most common method of H<sub>2</sub> production in chemical industries, where the steam reforming of natural gas accounts for approximately 95 % of the hydrogen produced in the United States.

In a study conducted by Piroonlerkgul et al. (2008), it was analyzed systems using different reforming agents, such as steam, air, and a mixture of steam and air, and it was found that steam was the most suitable agent, generating greater energy density than other air-powered systems; however, it presented a slight decline in electrical efficiency due to expenditures for generating steam. Table 2.3 compares the efficiencies and costs of the major technologies for hydrogen production:

**Table 2.3** Efficiencies and costs of major technologies for hydrogen production (Adapted from T-Raissi and Block 2004)

Process	Efficiency [%]	Costs associated with SRM
Steam reforming of methane (SRM)	70–80	1
Pyrolysis of methane/natural gas	72–54	0.9
Dry reforming of landfill gas	47–58	~1
Partial oxidation of heavy oils	70	1.8
Steam reforming of waste oil	75	<1
Coal gasification	60	1.4–2.6
Partial oxidation of coal	55	–
Water electrolysis using wind power	10	>3
Water electrolysis at high temperatures	48	2.2
Thermochemical water splitting	35–45	6
Biomass gasification	45–50	2.0–2.4

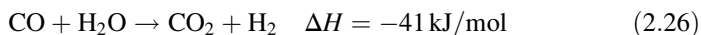
The reforming process occurs by feeding the system with biogas (syngas, natural gas, or pure methane), and then the superheated steam passes through a bank of tubes on a fixed-bed reactor with nickel as catalyst, thus generating  $H_2$  and  $CO$ , according to Eq. (2.25):



The thermodynamic equilibrium of this reaction depends on temperature, pressure, and steam-to-carbon molar ratio conditions, usually referred to as S/C ratio. The steam reforming reaction is strongly endothermic and favored by high temperature and pressure conditions. The reforming rates are controlled by the reaction kinetics, the gas's mass transfer rate to the surface of the catalyst, the diffusion rate through the pores of the catalyst, and the transfer of heat through the tubes of the reformer (Alves 2005).

Afterwards, the steam reforming products are directed to shift reactors, whose function is to reuse reagents that were not used in the steam reforming process, and the products of partial reactions that occurred in the reformer (such as  $CO$ ), producing additional  $H_2$ , as shown in Eq. (2.26).

Shift reaction:



Carbon monoxide ( $CO$ ), even in small concentrations, can be extremely harmful in certain fuel cell types. The overall steam reforming reaction is represented in Eq. (2.27):

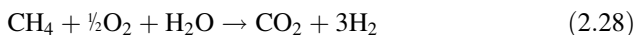
Overall reaction:



#### 2.2.3.4 Autothermal Reforming

Autothermal reforming is a combination of steam reforming and partial oxidation. It has aroused interest on account of removing the disadvantages of other reactions: low energy requirement to compensate for the effects of endothermic reactions (steam reforming) and exothermic reactions (partial oxidation). In addition, it presents low specific consumption, and there is effective control over the  $H_2/CO$  ratio by adjusting the feed rates of oxygen and steam (Cai et al. 2006).

There is great interest in this type of reforming process, especially for hydrogen production in small-scale applications, such as distributed generation and small stationary stations, due to its high efficiency, fast startup, and response (Araki et al. 2010). Equation (2.28) shows a typical autothermal reforming reaction.



## 2.2.4 Catalyst for Steam Reforming Reactions

As the steam reforming process is composed of catalytic reactions, the study of catalysts becomes an essential part in this chapter. The use of suitable catalysts can minimize unwanted reactions, such as Boudouard's reaction (Duane et al. 2002).

The greatest difficulty of reforming reactions to produce hydrogen and synthesis gas lies in obtaining stable catalysts, which are simultaneously selective for CO<sub>2</sub> and H<sub>2</sub> and resistant to metallic synthesis and coke deposition (Abreu et al. 2012). Two ways to minimize the formation of coke on the catalyst are highlighted as follows: by increasing the steam-to-carbon (S/C) molar ratio (Wang et al. 2004a, b) and the selection of a suitable medium, as well as its metallic phase and preparation method (Silva 2010).

### 2.2.4.1 Catalyst for the Steam Reforming of Ethanol

For this type of reforming process, two catalysts available in literature were selected, which work at different temperatures and have different conversion rates, which are presented in Table 2.4.

The catalyst 5 %Ni-5 %Cu/ $\gamma$ -Al<sub>2</sub>O<sub>3</sub> offers advantages in comparison with 20 %Ni/ $\gamma$ -Al<sub>2</sub>O<sub>3</sub> because it presents the best conversion rate and works at a lower temperature. Therefore, this catalyst was considered as the basis for the study of this kind of reforming process. It was also used in the prototype for the steam reforming of ethanol, developed by the Group of Optimization of Energy Systems.

### 2.2.4.2 Catalyst for the Steam Reforming of Natural Gas

For this kind of reforming process, two catalysts available in literature were also selected, which work at different temperature ranges and present different methane conversion rates as indicated in Table 2.5.

**Table 2.4** Catalysts for the system of steam reforming of ethanol (Adapted from Maia et al. 2007 and Liguras et al. 2003)

Catalyst/support	Reaction temperature (°C)	H <sub>2</sub> O/C <sub>2</sub> H <sub>6</sub> O	Ethanol conversion (%)
5 %Ni-5 %Cu/ $\gamma$ -Al <sub>2</sub> O <sub>3</sub>	400	5	97.62
20 %Ni/ $\gamma$ -Al <sub>2</sub> O <sub>3</sub>	700	3	77

**Table 2.5** Catalysts for the system of steam reforming of natural gas (Adapted from Souza 2005 and Beurden 2004)

Catalyst/support	Reaction temperature (°C)	H <sub>2</sub> O/CH <sub>4</sub>	Methane conversion (%)
15 %Ni/ZrO <sub>2</sub> - $\gamma$ -Al <sub>2</sub> O <sub>3</sub>	650	1	66
2 %Ru/ $\alpha$ -Al <sub>2</sub> O <sub>3</sub>	800	2.5	85



2 %Ru/ $\alpha$ -Al<sub>2</sub>O<sub>3</sub> achieves the best conversion rate, but it works at higher temperatures. According to literature, this high temperature condition is a typical feature of this kind of reforming process (Stein et al. 2009), thus it was opted for this catalyst as the basis for the study of the present reforming process.

### 2.2.4.3 Catalyst for the Steam Reforming of Biogas

For this type of reforming process, two types of catalysts were also selected, which are shown in Table 2.6 with their respective operating temperature and methane conversion rate.

5 % Ru/ $\gamma$ -Al<sub>2</sub>O<sub>3</sub> achieves the lowest conversion rate and works at a lower temperature. However, it was opted for this type of catalyst as the basis for the study of this reforming process because it is similar to the one chosen for the steam reforming of natural gas and, moreover, on account of having been used in the prototype built by the Group of Optimization of Energy Systems.

According to Avraam et al. (2010), it was observed that for CH<sub>4</sub>/CO<sub>2</sub> molar ratios greater than 1.5 and H<sub>2</sub>O/CH<sub>4</sub> of 2, the conversion rate of methane decreased slowly, becoming practically constant at 80 %.

### 2.2.4.4 Shift Reaction

The shift reaction, otherwise known as *water-gas shift reaction*, is the same in all reforming processes and occurs in a second reactor. It is an industrial technology in which steam (H<sub>2</sub>O) reacts with carbon monoxide (CO) to produce hydrogen (H<sub>2</sub>) and carbon dioxide (CO<sub>2</sub>), as presented in Eq. (2.26) (Haryanto, et al. 2011).

There are studies on catalysts for this process, but the most common one is shown in Table 2.7.

Thus, according to Table 2.7, it was opted for this catalyst as the basis for the study of the *shift* reaction. This was also the catalyst used in both shift reactor prototypes developed by the group of optimization of energy systems.

**Table 2.6** Catalysts for the system of steam reforming of biogas (Adapted from Aizquierdo et al. 2012 and Avraam et al. 2010)

Catalyst/support	Reaction temperature (°C)	CH <sub>4</sub> /CO <sub>2</sub> and H <sub>2</sub> O/CH <sub>4</sub>	Biogas conversion (%)
11.4 %Ni/ Zr- $\gamma$ -Al <sub>2</sub> O <sub>3</sub>	800	1.5 and 2	98.8
5 %Ru/ $\gamma$ -Al <sub>2</sub> O <sub>3</sub>	700	1.5 and 2	90.0

**Table 2.7** Catalyst for the water-gas shift reaction system (Adapted from Brenna 2010)

Catalyst/support	Reaction temperature	H <sub>2</sub> O/CO	Carbon monoxide conversion
Cu/ZnO/ $\gamma$ -Al <sub>2</sub> O <sub>3</sub>	250 °C	2	93 %

## 2.2.5 Experimental Analysis of the Steam Reforming of Ethanol

Considering the need to seek alternative energy sources, the potential of heterogeneous catalysis and the benefits obtained by the use of hydrogen, it was defined a methodology adopted for the experimental analysis of the steam reforming process proposed in this chapter, which consists in the investigation of technical aspects, such as preparation of mono- and bimetallic catalysts that are suitable for the steam reforming of ethanol, development of a method to characterize supports and catalysts, and, furthermore, conducting experimental tests on reforming prototypes with the capacity to produce 1 Nm<sup>3</sup>/h of hydrogen.

### 2.2.5.1 Pure and Mixed Supports, and Mono- and Bimetallic Catalysts Preparation

According to the characteristics of each material and behavior associated with the steam reforming reactions of ethanol, it was defined the composition and preparation methods of supports and catalytic series, which are composed of mono- and bimetallic catalysts (15 %Ni, 15 %Cu, 0.5 %Pt, 0.5 %Pt-15 %Ni). Figure 2.11 shows the sequence of experimental steps used in the preparation of catalytic materials.

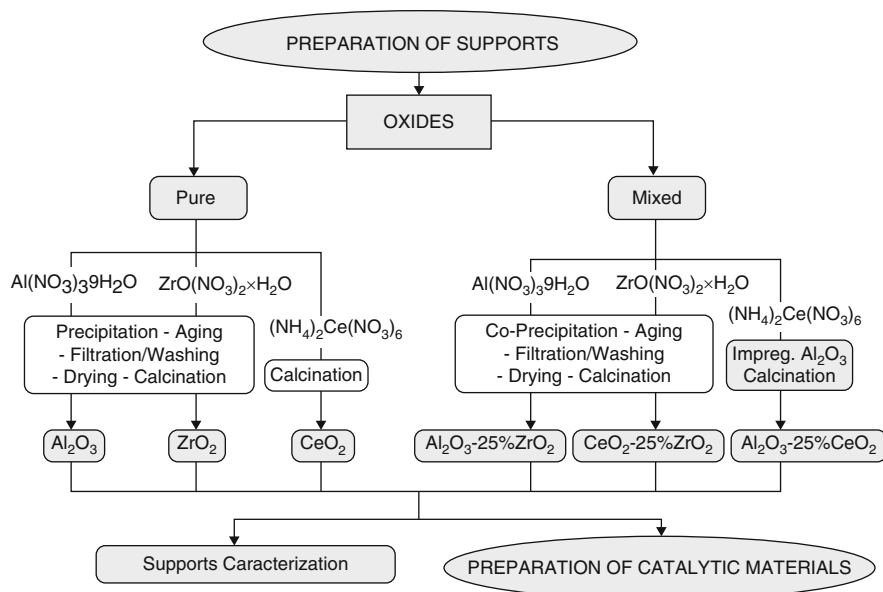


Fig. 2.11 Methods used in the preparation of catalytic materials

For each prepared support ( $\gamma\text{-Al}_2\text{O}_3$ ;  $\text{ZrO}_2$ ;  $\text{CeO}_2$ ;  $\gamma\text{-Al}_2\text{O}_3 - 25\%\text{ZrO}_2$ ;  $\gamma\text{-Al}_2\text{O}_3 - 25\%\text{CeO}_2$ ;  $\text{CeO}_2 - 25\%\text{ZrO}_2$ ), the precursor material and experimental method were employed that, according to the chemical composition of the oxide support and the characteristics observed by other researchers, would have more suitable properties to be used in the steam reforming of ethanol reactions. It can be observed in Fig. 2.11 that, in the preparation of pure oxides, experimental techniques involving precipitation, aging, filtration, washing, and heat treatments of drying and calcination were used. As for the preparation of the mixed oxides, in addition to the aforementioned techniques, the methods of coprecipitation and impregnation were used.

### *Materials and Reagents*

The mono- and bimetallic catalysts containing 15 %Ni, 15 %Cu, 0.5 %Pt, 0.5 %Pt-15 %Ni, supported on alumina ( $\gamma\text{-Al}_2\text{O}_3$ ), zirconium(II)oxide ( $\text{ZrO}_2$ ), ceria ( $\text{CeO}_2$ ), alumina-zirconia ( $\gamma\text{-Al}_2\text{O}_3\text{-}25\%\text{ZrO}_2$ ), alumina-ceria ( $\gamma\text{-Al}_2\text{O}_3\text{-}25\%\text{CeO}_2$ ), and ceria-zirconia ( $\text{CeO}_2\text{-}25\%\text{ZrO}_2$ ) were prepared by the dry impregnation method (also called incipient impregnation) and submitted to heat treatments of washing, drying, and calcination (Table 2.8).

### Preparation of Catalytic Supports

#### *Methods of Preparation: Pure Oxides*

The procedures for preparing the catalytic supports, which are pure aluminum oxide, Zirconium dioxide, and ceria oxide, are described below with the different

**Table 2.8** Materials and reagents

$\text{Al}(\text{NO}_3)_3 \cdot 9\text{H}_2\text{O}$	P.A. (98 %)	Sigma-Aldrich
$\text{ZrO}(\text{NO}_3)_2$	P.A. (99 %)	Sigma-Aldrich
$\text{Zr}(\text{OH})_4$	P.A. (97 %)	Sigma-Aldrich
$(\text{NH}_4)_2\text{Ce}(\text{NO}_3)_6$	P.A. ACS (98.5 %)	Sigma-Aldrich
$\text{Cu}(\text{NO}_3)_2 \cdot 3\text{H}_2\text{O}$	P.A. (99.999 %)	Sigma-Aldrich
$\text{Ni}(\text{NO}_3)_2 \cdot 6\text{H}_2\text{O}$	P.A. ( $\geq 97\%$ )	Sigma-Aldrich
$\text{H}_2\text{PtCl}_6 \cdot x\text{H}_2\text{O}$	P.A. (99.9 %—38 %Pt)	Sigma-Aldrich
$\text{NH}_4\text{OH}$	P.A. (28–30 % $\text{NH}_3$ )	Sigma-Aldrich
$\text{C}_2\text{H}_5\text{OH}$	P.A. ACS ( $\geq 99.5\%$ )	Sigma-Aldrich
$\text{HNO}_3$	P.A. ACS (63 %)	Sigma-Aldrich
$\text{HCl}$	P.A. ACS	Sigma-Aldrich
Argon 5.0 Analytical	(99.999 %)	White Martins
Helium 5.0 Analytical	(99.999 %)	White Martins
Ultra pure nitrogen		White Martins
Ultra pure hydrogen		White Martins
Primary standard mixtures		White Martins
$\text{H}_2\text{O}$		Distilled

heat treatments to which they were subjected, as well as a list of the different solids obtained with their respective nominal compositions and designations.

The prepared supports were:

- Aluminum oxide or alumina ( $\text{Al}_2\text{O}_3$ )
- Zirconium dioxide or zirconia ( $\text{ZrO}_2$ )
- Cerium oxide or ceria ( $\text{CeO}_2$ )

•  **$\gamma\text{-Al}_2\text{O}_3$**

The support  $\gamma\text{-Al}_2\text{O}_3$  was prepared by precipitation using solutions of aluminum nitrate  $\text{Al}(\text{NO}_3)_3 \cdot 9\text{H}_2\text{O}$  (0.5 mol/L) and ammonium hydroxide  $\text{NH}_4\text{OH}$  (6 mol/L). The precipitation consisted in dripping the aluminum nitrate solution (0.5 mol/L) evenly over the ammonium hydroxide solution (6 mol/L) with a peristaltic pump under constant stirring at  $\text{pH} \geq 10$ , as shown in Fig. 2.12.

Afterwards, the system became idle with the purpose of aging for 16 h at 298 K. After the aging process, the precipitate was filtered and washed in a Büchner funnel with distilled water at 333 K using the system presented in Fig. 2.13a for removing the precipitating agent until the washing water reached neutral pH.

Afterwards, the obtained aluminum hydroxide was dried in a Heraeus Vacutherm vacuum drying oven for 16 h at a temperature of 343 K, Fig. 2.13b. After being cooled in a desiccator, the material was ground and submitted to calcination in a Quimis muffle furnace at 773 K for 3 h, at a heating rate of  $10^\circ\text{C}/\text{min}$ , Fig. 2.13c.

**Fig. 2.12** Precipitation system





**Fig. 2.13** Equipments utilized: (a) Washing-filtration, (b) vacuum drying, and (c) calcination systems

- **ZrO<sub>2</sub>**

The support ZrO<sub>2</sub> was prepared by precipitation using solutions of zirconium oxynitrate (ZrO(NO<sub>3</sub>)<sub>2</sub>·xH<sub>2</sub>O) (0.2 mol/L) and ammonium hydroxide (NH<sub>4</sub>OH) (6 mol/L). The experimental procedures of precipitation, aging, filtering and drying, and calcination were similar to those described in the preparation of γ-alumina.

- **CeO<sub>2</sub>**

As for the preparation of the support CeO<sub>2</sub>, it was obtained by calcining the precursor Ceric ammonium nitrate (NH<sub>4</sub>)<sub>2</sub>Ce(NO<sub>3</sub>)<sub>6</sub> in a muffle furnace (Quimis) at 1073 K for 3 h, with heating control once room temperature was reached, at a rate of 10 °C/min. In this case, the heat treatment is responsible for decomposing the precursor salt for oxide phase determination.

### *Methods of Preparation: Mixed Oxides*

- **Al<sub>2</sub>O<sub>3</sub>-25 %ZrO<sub>2</sub>**

The mixed support γ-Al<sub>2</sub>O<sub>3</sub>-25 %ZrO<sub>2</sub> was obtained by coprecipitation with zirconium oxynitrate ZrO(NO<sub>3</sub>)<sub>2</sub>·xH<sub>2</sub>O (0.2 mol/L), ammonium nitrate nonahydrate Al(NO<sub>3</sub>)<sub>3</sub>·9H<sub>2</sub>O (0.5 mol/L), and ammonium hydroxide NH<sub>4</sub>OH (6 mol/L) solutions which were mixed and dripped over the ammonium hydroxide solution, according to the procedures used for obtaining γ-Al<sub>2</sub>O<sub>3</sub> and ZrO<sub>2</sub>, in which the coprecipitation, aging, filtering, drying, and calcination occurred.

- **Al<sub>2</sub>O<sub>3</sub>-25 %CeO<sub>2</sub>**

The mixed oxide Al<sub>2</sub>O<sub>3</sub>-25 %CeO<sub>2</sub> was obtained by dry impregnation of alumina Al<sub>2</sub>O<sub>3</sub>, using an aqueous solution of Ceric ammonium nitrate (NH<sub>4</sub>)<sub>2</sub>Ce(NO<sub>3</sub>)<sub>6</sub> as precursor, so as to obtain 25 % CeO<sub>2</sub> content (m/m).

- **CeO<sub>2</sub>-25 %ZrO<sub>2</sub>**

For the preparation of the mixed oxide CeO<sub>2</sub>-25 %ZrO<sub>2</sub>, it was used, in addition to the precursor Ceric ammonium nitrate solution (NH<sub>4</sub>)<sub>2</sub>Ce(NO<sub>3</sub>)<sub>6</sub> (0.01 mol/L), a solution of ZrO(NO<sub>3</sub>)<sub>2</sub>·xH<sub>2</sub>O (0.2 mol/L). The experimental procedure for preparing the support CeO<sub>2</sub>-25 %ZrO<sub>2</sub> was the same as that used for obtaining the mixed oxide γ-Al<sub>2</sub>O<sub>3</sub>-25 %ZrO<sub>2</sub>, in which the coprecipitation, aging, filtering, drying, and calcination occurred.

## Preparation of Promising Mono- and Bimetallic Catalysts for the Steam Reforming of Ethanol

The catalysts with nickel (Ni), platinum (Pt), copper (Cu), supported on alumina ( $\text{Al}_2\text{O}_3$ ), zirconia ( $\text{ZrO}_2$ ), ceria ( $\text{CeO}_2$ ), alumina-zirconia ( $\text{Al}_2\text{O}_3$ -25 % $\text{ZrO}_2$ ), alumina-ceria ( $\text{Al}_2\text{O}_3$ -25 % $\text{CeO}_2$ ), and ceria-zirconia ( $\text{CeO}_2$ -25 %  $\text{ZrO}_2$ ) were prepared by the dry impregnation method (also called as incipient impregnation) and submitted to washing and the heat treatments of drying and calcination, as shown in Fig. 2.14.

The supports were impregnated using aqueous solutions of nickel(II)nitrate hexahydrate  $\text{Ni}(\text{NO}_3)_2 \cdot 6\text{H}_2\text{O}$ , chloroplatinic acid hydrate  $\text{H}_2\text{PtCl}_6 \cdot x\text{H}_2\text{O}$ , and copper(II)nitrate trihydrate  $\text{Cu}(\text{NO}_3)_2 \cdot 3\text{H}_2\text{O}$  as precursors in order to obtain mono- and bimetallic catalysts with the following contents: 15 % nickel (m/m), 0.5 % platinum (m/m), 15 % copper (m/m), and 15 % nickel-platinum Ni-0.5%Pt(m/m).

The volume of the impregnating aqueous solution is equal to the total porous volume of the support, i.e., it corresponds to the mass of the one that is going to be impregnated ( $V_{\text{solution}} = V_{\text{total porous}} = P_v \times \text{mass}$ ).

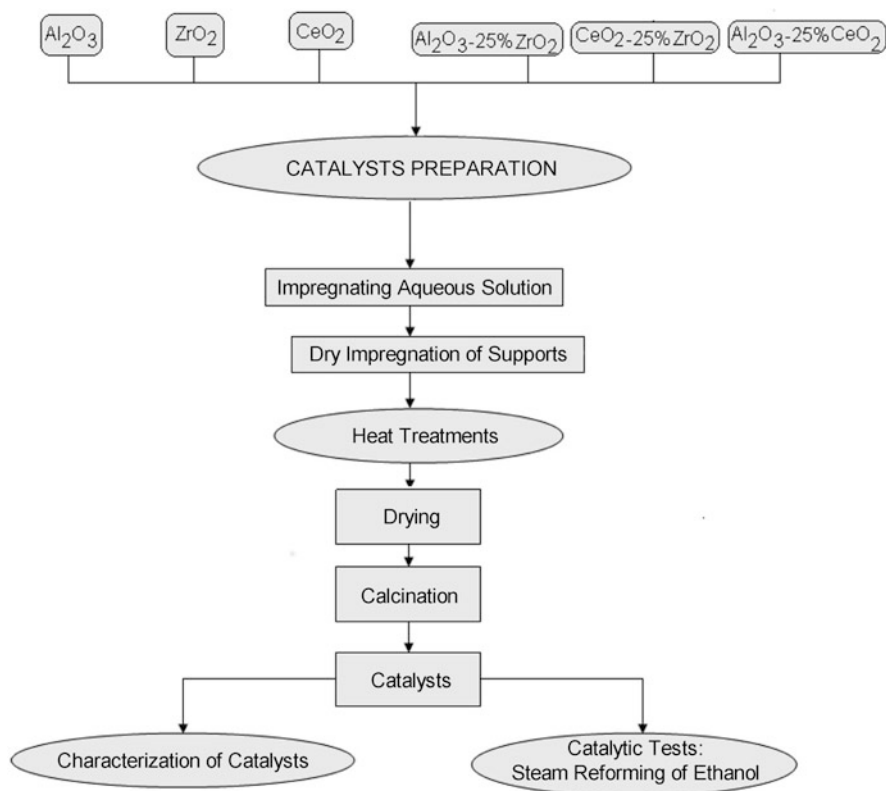


**Fig. 2.14** Catalysts preparation method

**Fig. 2.15** Illustration of the system used for the dew point determination



Specific porous volumes ( $P_v$ ) were determined by the dew point method, as shown in Fig. 2.15. This method consists in determining the absorption capacity of a liquid by moisturizing the support in the form of powder until it becomes wet, i.e., before clusters or a paste is formed.

Distilled water was used as liquid, which was inserted in a 10 mL automatic pipette. The water was dripped slowly and mixed with the support with a glass rod in a beaker until the dew point could be visualized. The support mass was 1 g, and at least three measurements of the absorbed liquid volume were made. Thus, the average value obtained was considered as the specific porous volume.

After impregnation, the catalysts were dried in a vacuum oven for 16 h at a temperature of 343 K (Fig. 2.13b), and then submitted to calcination that was conducted with heating control once room temperature was reached at a rate of 10 °C per minute (10 °C/min) until reaching 773 K. The calcination was performed in a muffle furnace (Quimis) for 3 h at 773 K (Fig. 2.13c) for removing water and heat stabilization.

### **2.2.6 Methods for the Characterization of Supports and Catalysts**

The characterization of a catalyst results in three distinct, but interrelated pieces of information, which are: composition or chemical structure, textural properties and catalytic behavior. In principle, one should consider that almost any method of analysis related to materials science has enough potential to be used for catalyst characterization. However, experience has revealed that only a relatively restricted number of techniques are fundamentally important to catalysis sciences.

**Table 2.9** Most commonly used methods to characterize catalysts

Proprieties	Characterization methods
Porosity, porous volume	Pycnometry, liquid absorption
Specific surface area	BET method
Metal specific surface area	Gas volumetry (H <sub>2</sub> , CO)
Support crystallinity	XRD
Elemental composition	EDX
Chemical composition	AAS
Activity, selectivity	Kinetic analysis

Nevertheless, the field is extremely extensive and there are situations where there is more than just one technical alternative available to assess a particular property. The most commonly used methods that are already relatively standardized are summarized in Table 2.9.

The various characterization techniques employed for studying the prepared catalytic materials were selected from the need to better understand their physico-chemical properties and to analyze some of the most commonly used techniques in the study of the species present in a catalyst, as listed:

- Specific surface area—(BET method)
- Atomic Absorption Spectrometry—(AAS)
- Energy-dispersive X-ray spectroscopy (EDX or EDS)
- X-ray diffraction (XRD)
- Catalytic Tests involving the cyclohexane dehydrogenation Reaction

## 2.2.7 *Considerations on the Characterization of Catalytic Materials*

Therefore, for characterizing the prepared catalytic supports, it should be conducted conduct specific surface area analyses (BET), a crystallinity analysis by X-ray diffraction (XRD), and a metal content analysis of the mixed oxides through energy-dispersive X-ray spectroscopy (EDS). As regards the catalysts characterization, it should be carried out an elemental analysis by atomic absorption spectrometry, Energy-dispersive X-ray spectroscopy (EDS), Atomic Absorption Spectrometry (AAS), crystallinity analysis by X-ray diffraction (XRD), and assessments of a model reaction, such as a catalytic test of the cyclohexane dehydrogenation reaction.

The catalysts activity is generally assessed by bench tests, i.e., bed quartz microreactors at atmospheric pressure are used, which are set according to the characteristics of the reaction system adopted for the catalytic tests of the series of catalysts. The products of the heterogeneous steam reforming reaction are identified and quantified by gas chromatography.

The characterization of the prepared catalysts will, in future works, contribute to the investigation of the most promising series for applications in ethanol steam



reformers by a comparison with the behavior of 6 %Ni-6 %Cu supported on commercial alumina ( $\gamma\text{-Al}_2\text{O}_3$ —Oxiteno,  $200\text{ m}^2\text{ g}^{-1}$ ;  $0.03\text{ m}^3\text{ g}^{-1}$ ; pellets) to be used in experimental trials carried out with the prototype for the steam reforming of ethanol.

However, from the experimental results obtained with the reforming prototype, economic and ecological analyses of the developed reforming prototype will be conducted so as to determine the cost-benefit relations of the proposed steam reforming system, and the ecological efficiency of hydrogen production generated by the reformer.

### 2.2.8 *Prototype for the Steam Reforming of Ethanol*

Reformers are devices that process ethanol into a synthesis gas which is rich in hydrogen. After that, the syngas is subjected to a purification step to meet the requirements of its application. The main components of the ethanol steam reformer are: a metering pump, a water vaporizer, a steam reforming reactor, and a water-gas shift reactor. The metering pump feeds the liquid mixture (water and ethanol) and the vaporizer, in turn, gasifies the fuel mixture (anhydrous ethanol) and water to feed the first water-gas shift reactor, i.e., the reformer, which is a stage that occurs at high temperatures where the steam reforming reactions take place in order to form a hydrogen-rich gas mixture. Then, this gaseous mixture is subjected to a catalytic process of the shift reactor that removes part of the CO and produces additional hydrogen for the synthesis gas of the process. Figures 2.16 and 2.17 show the prototypes I and II, respectively, for the steam reforming of ethanol.

It can be observed in Fig. 2.16 a scheme depicting the components of the system of hydrogen production via the steam reforming of ethanol, followed by a purification system of the syngas operating with two columns in PSA cycles (Pressure Swing Adsorption). The hydrogen-rich syngas is subjected to a system of

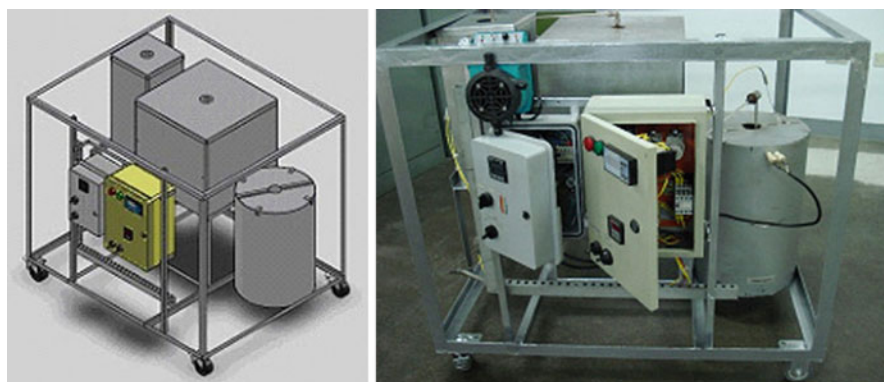


**Fig. 2.16** Ethanol reformer: Prototype I

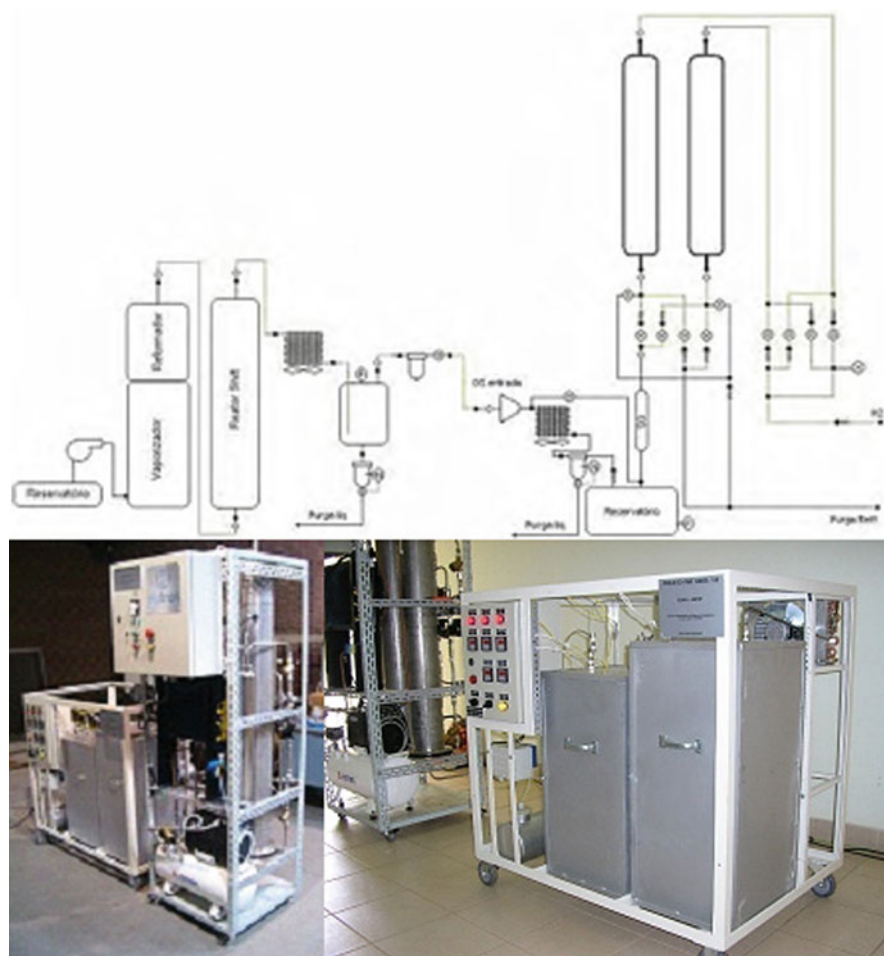


**Fig. 2.17** Ethanol reformer: Prototype II

purification by molecular adsorption (PSA) after the steam reforming process, so as to minimize the impurities, mainly the amounts of CO.

Figure 2.18 shows the proposed system for the steam reforming of ethanol associated with the fuel cell technology. According to fuel cell technologies and the characteristics of the steam reforming system, it is possible to carry out a joint operation of the steam reforming process with various types of fuel cells.

The qualification and quantification of the products derived from the steam reforming of ethanol process by using the reforming prototype were determined by gas chromatography using the Varian CP-4900 Micro-GC, Fig. 2.19. The gas chromatograph was set to operate with three independent channels to ensure the analysis of the components present in the syngas from the steam reforming process, as shown in Table 2.10.

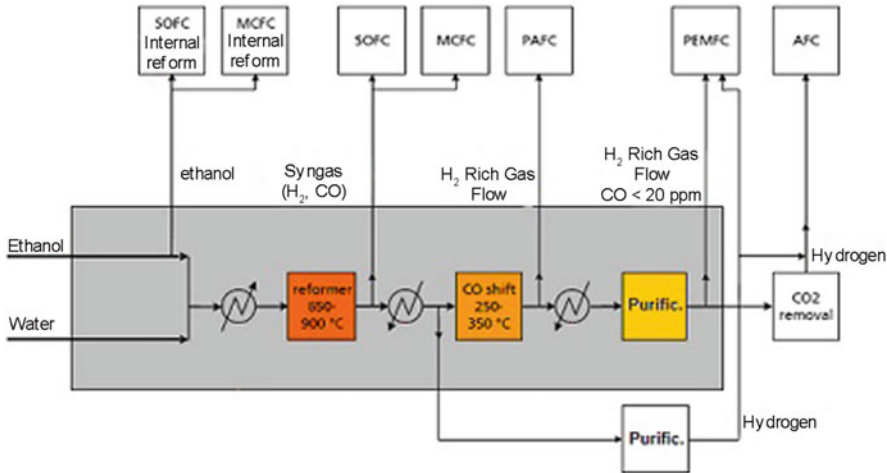


**Fig. 2.18** System of steam reforming of ethanol and fuel cell technologies (Adapted from Aiche 2005)



**Fig. 2.19** CP-4900 Micro-GC for gas analyses

**Table 2.10** Chromatograph settings

Micro GC CP-4900 settings			
Hardware	Channel 1	Channel 2	Channel 3
Carrier gas	Helium	Argon	Argon
Injector	Heated	Heated	Heated
Column	PPU	Cp sil 5	Molesieve 5A
Separation	Ar; CH <sub>4</sub> ; C <sub>2</sub> H <sub>4</sub> ; H <sub>2</sub> O; H <sub>2</sub> S	Alcohols and aldehydes	H <sub>2</sub> ; Ar; O <sub>2</sub> ; N <sub>2</sub> ; CO; CH <sub>4</sub>
Backflush	NO	NO	YES
Eliminated components	N/a	N/a	CO <sub>2</sub> ; H <sub>2</sub> O; Hydrocarb.

**Table 2.11** Operation parameters of the system

System component	Operation parameter
Vaporizer	Water/ethanol volume ratio: (1–0.9)
	Generated gas temperature: 923 K
Reformer	Catalyst: 6 %Ni-6 %Cu/ $\gamma$ -Al <sub>2</sub> O <sub>3</sub>
	Reaction temperature: 923 K; 1 atm
Water-gas shift reactor	Catalyst: Cu/ZnO/ $\gamma$ -Al <sub>2</sub> O <sub>3</sub>
	Reaction temperature: 493 K; 1 atm
Purificator	Adsorbent bed: PSA cycles
	Gas feed flow rate: 25 L/min, 0.4 bar
	Feed temperature: 313 K (max)
	Inlet pressure: 0.6 bar
	Working pressure: 6.5 bar

### 2.2.8.1 Experimental Trials with the Steam Reforming of Ethanol Prototype

Experimental trials were conducted with the reforming prototype. However, before the catalytic tests involving Ni-Cu/Al<sub>2</sub>O<sub>3</sub> and Cu-Zn/Al<sub>2</sub>O<sub>3</sub>, their H<sub>2</sub>/N<sub>2</sub> flow rate was reduced to 773 K and 503 K, respectively. Table 2.11 shows the operation parameters of the system components.

### 2.2.8.2 Catalyst Activation in the Steam Reforming Prototype

The catalysts were reduced, in situ, in order for the catalytic surface to be active, and so that it is no longer oxidated on account of air exposure, and especially due to the high temperatures reached during the calcination period. Figure 2.20 shows the steam reformer during the experimental trial of catalyst activation.

Initially, the purification of the steam reforming reactors was performed with an inert gas, e.g., argon, until all oxygen was removed. The inert gas flow through the reactor was set to a given speed in order to ensure good flow distribution in the catalytic beds. After purification, the catalytic beds heating started under inert gas flow at a rate of about 323 K/h until the temperature of 423 K was reached. Afterwards, the inert gas flow was increased and the catalysts were heated to a bed top temperature of 443 K.

After a temperature of 573 K was reached in the water-gas shift reactor, about 0.5 % hydrogen was added to the inert gas flow, but not exceeding 1.0 vol.% so that no point of the bed exceeds the temperature of 723 K in the reformer, and 503 K in the water-gas shift reactor.



**Fig. 2.20** Steam reforming of ethanol prototype: catalyst reduction

**Table 2.12** Synthesis gas analysis result—before and after purification

Samples	H <sub>2</sub> (%mol/mol)	CO (%mol/mol)	CH <sub>4</sub> (%mol/mol)	CO <sub>2</sub> (%mol/mol)
Synthesis gas—reformer	75.24	8.64	6.79	8.12
Synthesis gas—reformer/purificator	99.84	<1.0	<1.0	<1.0

### 2.2.8.3 Ethanol Reformer: Prototype

Table 2.12 shows the results of the chromatographic analysis of the syngas obtained in the experimental trials of the steam reforming of ethanol system, reforming prototype II. It can be observed a high yield of hydrogen production, and low concentrations of CO, CH<sub>4</sub>, and CO<sub>2</sub>, which suggests that the reforming and water-gas shift reactions were strongly favored by temperature conditions of 923 K and 493 K, respectively.

Moreover, the results of the synthesis gas, collected after the purification system by molecular adsorption PSA (Pressure Swing Adsorption), show a hydrogen-rich gas flow, i.e., 99.84 % mol/mol of H<sub>2</sub> and low CO, CH<sub>4</sub>, and CO<sub>2</sub> mol/mol percentages. The hydrogen-rich syngas flow obtained after the purification system allows using the produced hydrogen as input to generate electricity in PEM fuel cells.

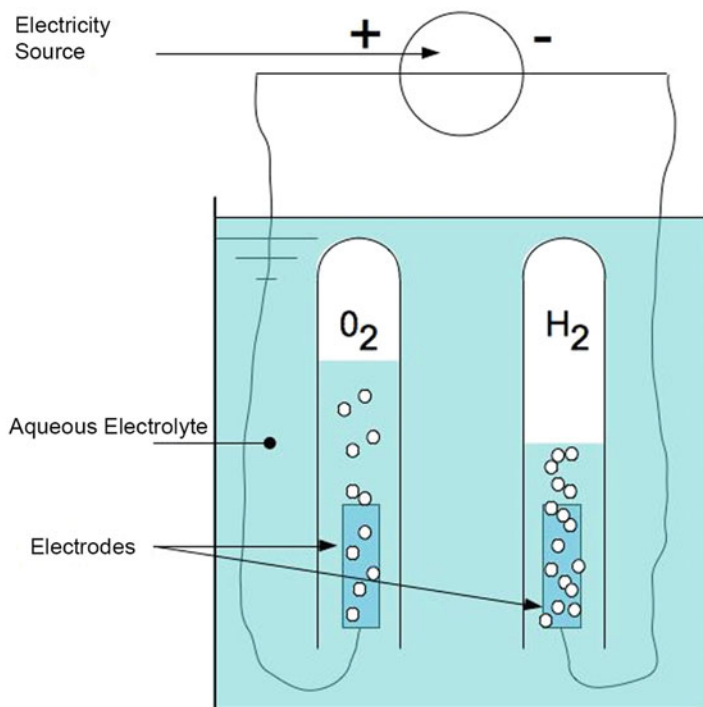


**Fig. 2.21** Electrolysis process scheme (Reproduced from Hy Generation [2014](#))

### 2.3 Hydrogen Production by Water Electrolysis

Figure [2.21](#) illustrates a simple scheme of an electrolysis process.

The electrolysis process consists, essentially, of an electricity source (direct current), electrodes (anode and cathode), and a conductive electrolyte. Both in acid and basic electrolytes, oxidation occurs in the anode and reduction in the cathode, with a subsequent hydrogen production. The difference is in the species involved in the oxidoreduction process: on the one hand, protons ( $H^+$ ) are involved, and on the other one, the hydroxyl ions ( $OH^-$ ).

There are a few hindrances to the electrolysis process. One of them is the fact that a large amount of thermal energy is required to split the water molecule. It is estimated that the amount of energy required to perform the electrolysis is the same as that provided by hydrogen production. Therefore, by considering the dissipation of energy, it takes more energy to perform the electrolysis than the amount that it can generate (Lopez [2004](#)). However, with hydrogen being used as energy input, the process becomes feasible, as it uses renewable sources for generating the energy required for the process.

The positive and negative electrodes are separated by a microporous diaphragm, which currently replaces the previously used asbestos diaphragms (Sorensen [2005](#)).

The hydrogen ions are transported through the electrolyte due to the difference of electric potential. The alkaline component function is to improve the low ionic conductivity of water. However, this process is limited by temperatures below 100 °C in order to avoid a significant increase in the alkaline corrosion of the components (Sorensen 2005).

### 2.3.1 Electrolyzers

Conventional electrolyzers use an alkaline electrolyte solution as ionic conductor (aqueous potassium hydroxide). The electrodes are made of conventional materials, such as steel and carbon, and their anode surface is protected by traditional nickel plating (matte nickel), in order to avoid corrosion. Their operating temperature ranges from 70 to 80 °C, yielding between 70 and 80 % (Basso et al. 2013).

There are two forms of arranging electrodes in a conventional cell, which are the unipolar ones (tank type electrolyzers) and bipolar ones (filter-press electrolyzers), as shown in Figs. 2.22 and 2.23.

As for the unipolar electrolyzer, the conduction is made with the electrodes being arranged parallelly while, in the case of the bipolar electrolyzer, they are arranged serially (with the exception of those on the extremities) with one electrode working as anode in a cell and another one as cathode in the subsequent one. In the case of the unipolar electrolyzer, the electrolyte is ordinary, while it is individual in the bipolar electrolyzer (Silva 1991).

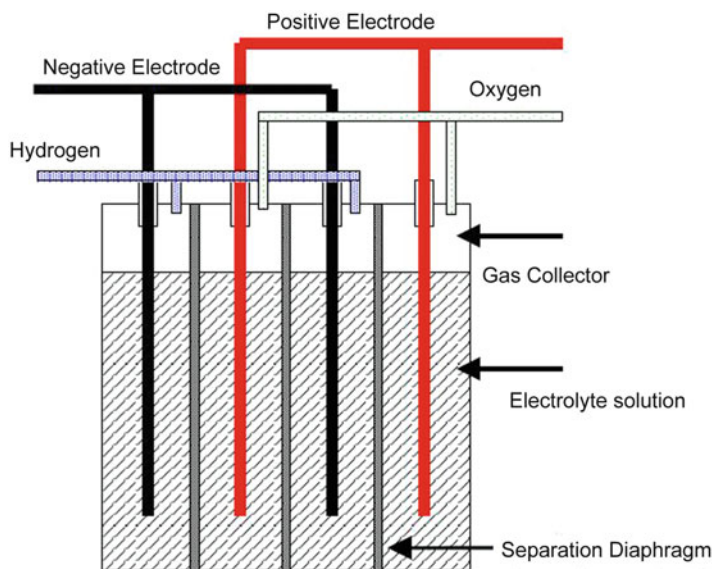
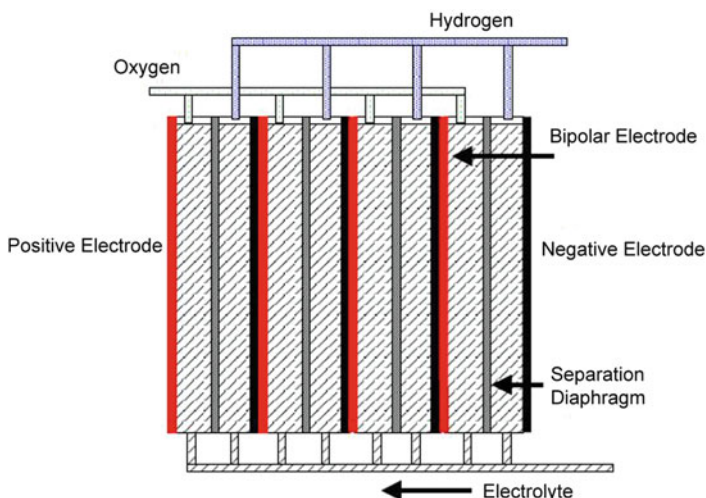


Fig. 2.22 Unipolar electrolyzer (Adapted from Kroposki et al. 2006)





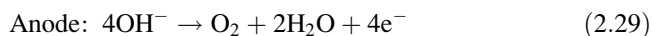
**Fig. 2.23** Bipolar electrolyzer (Adapted from Kroposki et al. 2006)

Monopolar electrolyzers are simpler and their maintenance is easier than that of bipolar electrolyzers, resulting in a lower cost per unit area in the cell. These electrolyzers are generally used for  $\text{H}_2$  production of up to  $100 \text{ Nm}^3/\text{h}$ , while bipolar electrolyzers are usually used for over  $100 \text{ Nm}^3/\text{h}$   $\text{H}_2$  production (Carnieletto et al. 2011).

Modern electrolyzers are similar to conventional models, but the electrodes are covered with special coatings, catalysts deposition, and rough surfaces. Some models use membranes separated by Teflon or other materials, and can be operated at temperatures ranging from  $80$  to  $120^\circ\text{C}$  and yields of  $80\text{--}90\%$  (Carnieletto 2011).

## 2.4 Alkaline Electrolysis (AEL)

From a technological point of view, alkaline electrolyzers are sufficiently well developed and ready to produce renewable hydrogen at significant rates. The equipment is reliable and secure, with total lifetime of up to 30 years, electrode and membrane exchange at every 8 years, operation efficiency ranging between  $62$  and  $82\%$ , and production capacity from  $1$  to  $760 \text{ Nm}^3/\text{h}$  (Smolinka et al. 2011). It consists mainly of two electrodes immersed in an aqueous solution of  $\text{KOH}$  or  $\text{NaOH}$  ( $25\text{--}30\%$ ). Hydrogen is produced at the cathode and oxygen at the anode. The reactions involved in the process are as follows:





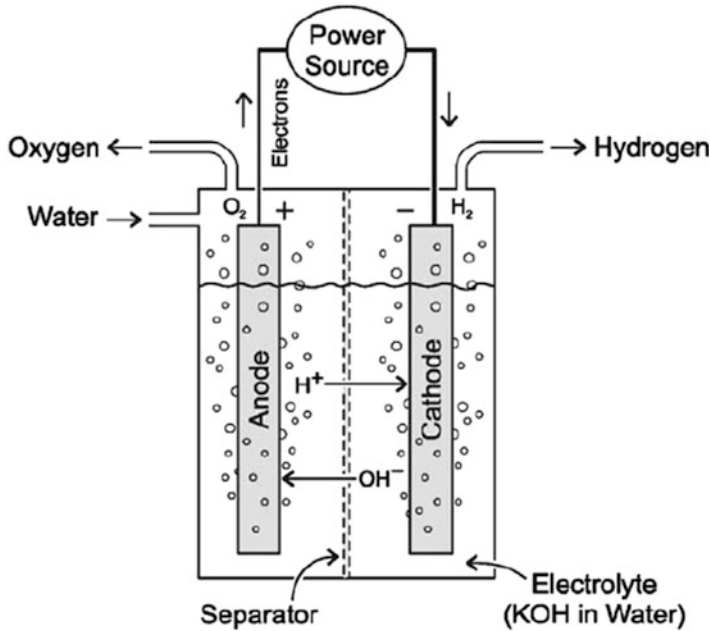
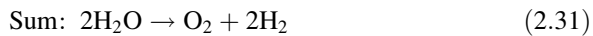


Fig. 2.24 Alkaline electrolyzer scheme (Adapted from Koroneos et al. 2004)



The electrodes are separated by a microporous membrane which is permeable to  $\text{OH}^-$  ions, but impermeable to gases. The anode is usually made of Nickel or Nickel-coated steel, while the cathode is made of steel coated with different catalysts. The distance between the electrodes is up to 5 mm and the operating temperature is usually limited to 80 °C (Bhandari et al. 2014). Figure 2.24 shows a scheme of the working principle of an alkaline electrolyzer.

There are alkaline electrolyzers operating at low pressures (up to 6 bar) and also at high pressures (from 6 to 30 bar). The advantage of operating at high pressures is that there is no need for a posterior compression of the produced hydrogen, although high pressures reduce the purity of the product due to increased permeability of the membrane in comparison with gases (Bhandari et al. 2014).

The alkaline electrolyzers' energy demand depends on the designing characteristics of the electrodes and their operating conditions. At low pressures, the specific energy demand is between 4.1 and 4.5 kWh/Nm<sup>3</sup>H<sub>2</sub>, sometimes reaching 7 kWh/Nm<sup>3</sup>H<sub>2</sub> due to compression. For pressurized electrolyzers, the specific energy demand is between 4.5 and 5 kWh/Nm<sup>3</sup>H<sub>2</sub> (Smolinka et al. 2011).

Improvements in technology have followed two directions. The first one consists in improving the electrolyzer efficiency in order to reduce operating costs

associated with electricity consumption. The second one aims to increase the operating current density to reduce investment costs. This situation is most evident in the case of large units in which investment costs are nearly proportional to the surface area of electrolytic cells (Ursúa et al. 2012). Investment costs are widely ranged between \$1000 and 2300€/kW (Bertuccioli et al. 2014).

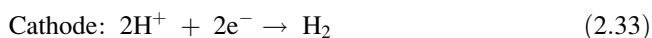
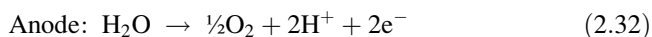
The alkaline electrolyzer has evolved over time. According to Ursúa et al. (2012), a few improvements were:

- Minimizing the space between the electrodes, reducing ohmic losses, and allowing operation with stronger currents.
- Developing new materials to be used as diaphragms instead of asbestos. In this case, the use of ionic-exchange inorganic membranes has been widely developed. Some examples are polyacid antimony membranes impregnated with polymers, porous composite compounds with a polysulfone and ZrO<sub>2</sub> (Zirfon) matrix, besides polyphenyl sulfide-based splitters (Ryton).
- Development of high-temperature electrolyzers. Operating temperatures above 150 °C increase the conductivity of the electrolyte and promote the kinetics of the electrochemical reaction under the surface of the electrode. These electrolyzers are intended for producing hydrogen on a large scale, reaching purification levels of up to 99.9 % (Ivy 2004).
- Development of advanced electrocatalyzing materials to reduce the electrode's overvoltage.

Alkaline electrolysis is a mature technology. Several manufacturers like Hydrogenics, Mcph, Teledyne Energy Systems, among others, have been selling this technology.

## 2.5 Electrolysis in Acid Medium (PEM Electrolysis)

Known as Proton Exchange Membrane (PEM) or Solid Polymer Electrolyte (SPE) electrolysis, this technology differs from alkaline electrolysis due to the fact that it does not require any electrolytic liquid. In this case, a thin splitting polymer membrane is used, allowing a close proximity of the electrodes. The membrane used in this device is Nafion<sup>®</sup>, developed by Dupont, which are less than 0.2 mm thick (Ursúa et al. 2012). The electrodes are composed of noble metal alloys, such as Platinum and Iridium. The chemical reactions that occur in a PEM electrolyzer are as follows:



At the anode, the water is oxidized for producing oxygen, protons, and electrons. The protons pass through the membrane to the cathode where they are transformed

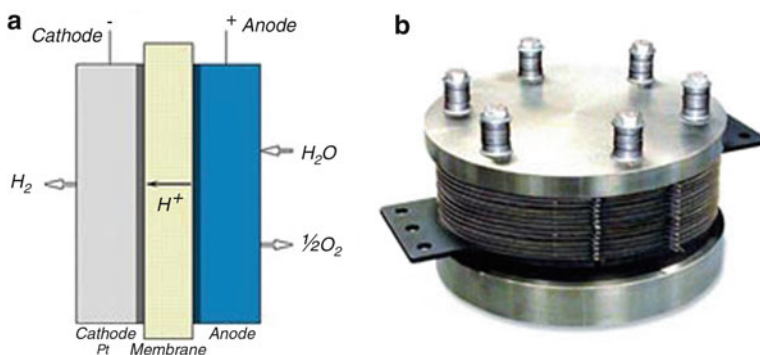


**Fig. 2.25** (a) PEM electrolyzer operation and (b) commercial-type electrolysis battery

into high purity hydrogen, typically over 99.99 % purity. The operating temperature is 80 °C at a pressure of up to 15 bar. The specific energy demand of PEM electrolyzers is between 4.5 and 7.0 kWh/Nm<sup>3</sup>H<sub>2</sub>, with production capacity ranging between 0.06 and 30 Nm<sup>3</sup>H<sub>2</sub>/h and operation efficiency ranging from 67 to 82 % (Smolinka et al. 2011; Ursúa et al. 2012).

PEM electrolyzers have emerged to circumvent some difficulties that the alkaline solution presents, such as the significant increase in the corrosion of electrodes (Sorensen 2005). They are not very sensitive to the effects of fluctuations in power supply, which makes them suitable for being applied to energy storage from renewable sources, unlike alkaline electrolyzers which have their efficiency compromised by presenting large inertia in transporting ions (Bhandari et al. 2014). The main problem is the high investment cost associated with the membranes and noble metals of electrodes. It is a technology which is still under development, but there are already several manufacturers, such as ITM Power, ProtonOnSite, and Siemens.

Figure 2.25a illustrates the operation of such electrolyzer and Fig. 2.25b shows a commercial-type electrolysis battery.

## 2.6 High Temperature Electrolysis (HTEL or SOEL)

SOE electrolyzers (solid oxide electrolyzers) perform electrolysis at high temperatures (600–1000 °C), enabling greater efficiencies than alkaline and PEM models, once the required power supply plummets. However, this process is hindered by the difficulty in finding thermally stable and waterproof materials that can last for a long period of time. The process basically consists in a solid oxide fuel cell working in reverse mode, where water vapor is introduced into the cathode at a high temperature which is reduced to produce hydrogen, and oxide anions are generated and pass through the solid electrolyte to the anode, where they are recombined to

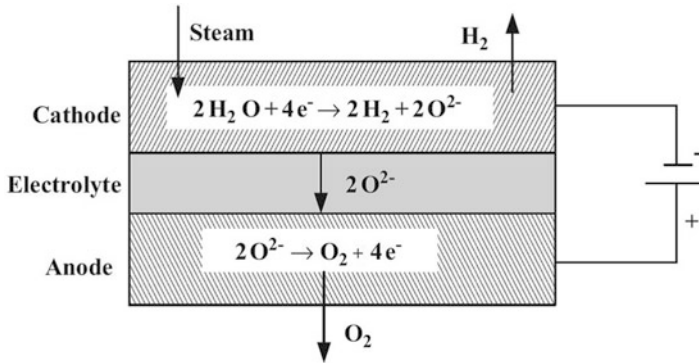


**Fig. 2.26** Operation of a solid oxide electrolyzer (Adapted from Wang et al. 2014)

form oxygen. The cathode consists of a hard metal with hard nickel-base particles with yttrium and zirconia (YSZ), where the electrolyte is a solid made of YSZ and the anode is made of perovskite ( $\text{CaTiO}_3$ ) (Ursúa et al. 2012). This kind of electrolyzer reduces the required power supply in up to 25 % by using heat from the process that occurs at 1000 °C (Brisse et al. 2008). This feature makes the SOE attractive for producing hydrogen when a high-temperature heat source is available, such as those from nuclear reactors, geothermal energy, and solar thermal energy. Currently, this type of electrolyzer is in its research phase and under development (Bhandari et al. 2014). It is expected that it will be commercially available in 3–5 years at an estimated cost of 2000 €/kW (Bertuccioli et al. 2014). Figure 2.26 shows the diagram of the process.

## 2.7 Renewable Electricity Sources for Electrolysis

### 2.7.1 Wind Power

Wind power is mainly produced from solar radiation, since winds are generated by a nonuniform heating of the Earth's surface. According to Dutra (2008), an estimate of the total wind power available around the planet can be made from the hypothesis that approximately 2 % of the solar energy absorbed by the Earth is converted into kinetic energy of winds. This percentage, though it seems small, represents hundreds of times the annual installed power of electricity plants worldwide.

According to the *International Renewable Energy Agency* (Irena et al. 2013), on account of technological advances in wind turbines, the cost of wind power in Latin America has varied from 0.05 to 0.17 US\$/kWh over the past few years.

However, the cost of wind power generation is more expensive in Latin America than in other countries that have adopted measures to encourage the construction of wind farms, like Germany, Spain and Denmark. This can be attributed to higher

logistic costs for implementing the projects and to the limited number of domestic suppliers of wind turbines, which can be associated with import restrictions on such instruments (Dantas and Leite 2013). The winds that blow on a global and small scale are influenced by different aspects, among which height, roughness, obstacles, and features of the terrain upon which the wind farm was built stand out (Dutra 2008).

According to Furlan (2012), the available wind power is the kinetic energy associated with the air mass traveling at a uniform and constant speed through the wind turbine, which can be calculated according to Eq. (2.34):

$$P_{\text{disp}} = \frac{1}{2} \rho_{\text{ar}} A v^3 \quad (2.34)$$

where:

$P_{\text{disp}}$ —power of wind turbine (W)

$\rho_{\text{air}}$ —air density ( $\text{kg}/\text{m}^3$ )

$A$ —cross-sectional area of the wind turbine ( $\text{m}^2$ );

$v$ —wind speed (m/s)

Once the speed at which the air mass is traveling is reduced, the kinetic energy of the wind is converted into mechanical energy through the rotation of the blades. However, the available wind power cannot be fully harnessed by the wind turbine in the conversion of electrical energy. The power that is effectively harnessed by a wind turbine's blades depends on the energy difference between the upstream and downstream of the rotor blades, as shown in Fig. 2.27 (Roberts 2012).

According to Fig. 2.27, generally speaking, it can be considered, under a macroscopic point of view, that wind speed varies from  $V$  to  $V_0$  on the plane of the rotor, with an average speed of  $\frac{1}{2}(V + V_0)$  at this flow rate. After a few algebraic operations, it can be determined the mechanical power obtained by the rotor, as shown in Eq. (2.35) (Roberts 2012).

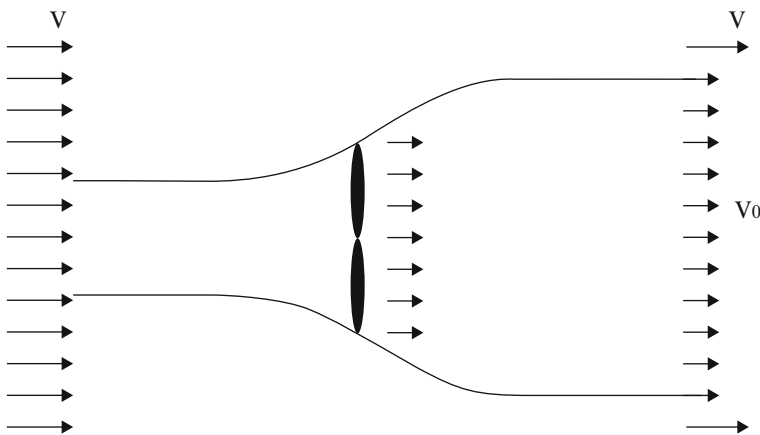


**Fig. 2.27** Loss of wind speed in a wind turbine (Adapted from Roberts 2012)

$$P_{mec} = \frac{1}{2} \rho_{ar} A v^3 c_p \quad (2.35)$$

where:

$P_{mec}$ —mechanical power of wind turbine (W)

$c_p$ —power coefficient

The concept of power coefficient was introduced by Betz law. The Betz limit indicates that, even when harnessing the most wind power, only a maximum of 59 % can be recovered, which indicates that the maximum  $c_p$  (theoretical) is approximately 0.59. According to Roberts (2012), in practice, the maximum efficiency achieved by modern wind turbines ranges from 0.2 to 0.4; the amount of energy that could not be harnessed is dissipated in the downstream wind.

The energy generated in this particular case of electrolysis can be used when there are winds with an average speed of 6 m/s and a minimum speed of 4 m/s (Silveira 2012). Figure 2.28 shows an eolic system that supplies the network with power, in addition to feeding an electrolyzer for hydrogen production.

As illustrated in Fig. 2.28, the hydrogen produced by the electrolyzer is directed to a storage system. The stored hydrogen can be either used in stationary fuel cells to produce electricity for the network, or in vehicular fuel cells of cars or buses.

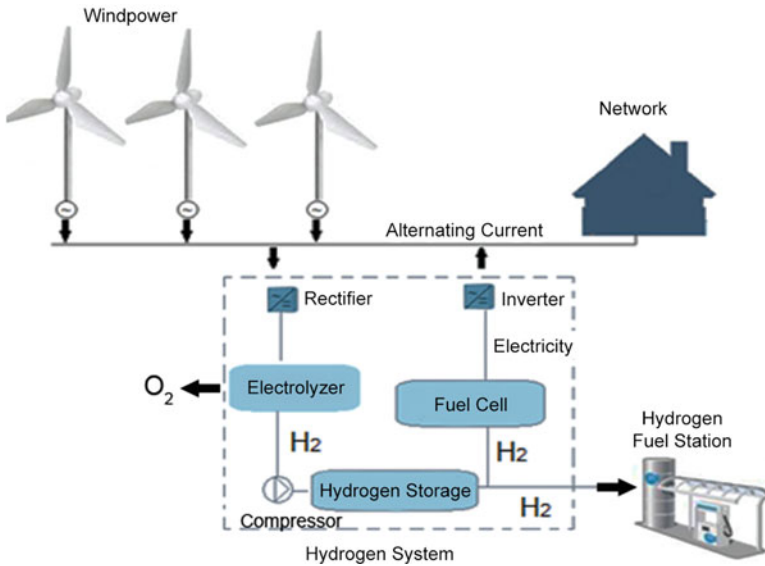


Fig. 2.28 Hydrogen production from wind power

### 2.7.2 Solar Power

Solar power is the electromagnetic energy from the sun, which is generated via nuclear reactions that, by being propagated through interplanetary space, is emitted onto the Earth's surface. Most other renewable energy sources also depend on the sun as primary source, such as hydroelectric, wind, and tidal power (Roberts 2012). The total solar energy emitted to the Earth's surface yearly is over 10,000 times the annual gross energy consumed by humanity (CRESESB 2012).

According to Silveira (2012), in the Brazilian territory, there is an average solar radiation of  $900 \text{ W/m}^2$ . A photovoltaic power plant converts  $80\text{--}180 \text{ W/m}^2$  of this amount into electricity (depending on the type of photovoltaic panel) during 6 h of the day (project parameter, which depends on the position of the sun). You must, however, use banks of batteries to store electricity to be used in periods in which the radiation cannot be harnessed, which pushes up the costs of investment in photovoltaic plants.

The materials used for manufacturing photovoltaic panels are semiconducting elements, where most of them are, on a commercial scale, made of silicon, which are also found in their monocrystalline, multicrystalline or polycrystalline, and amorphous forms (CRESESB 2012). According to Roberts (2012), this preference is due to three factors: silicon is nontoxic and the second most abundant element found in nature, whose technology is fully established.

A single photovoltaic cell generates between 1 and 1.5 W, at a voltage of 0.5–0.6 V, under standard trial conditions (solar radiation of  $1 \text{ kW/m}^2$ , cell temperature of  $25^\circ \text{C}$ , and air mass of 1.5 t). In order to obtain voltage and current levels that are suitable to their use, photovoltaic cells are usually arranged serially. Such setup, generally comprising 30 and 36 cells, constitutes a photovoltaic module (Roberts 2012).

The conversion efficiency of photovoltaic cells is measured by the amount of solar radiation that is emitted onto the surface of the cell, which is converted into electrical energy. Table 2.13 shows the efficiencies of photovoltaic panels.

It can be observed in Table 2.13 that the efficiency of photovoltaic panels is 14 % on average, which is relatively low in comparison with the energy generated by wind and hydroelectric turbines.

Solar hydrogen production systems are composed of a set of panels that supply an electrolyzer with direct current electricity. According to Gibson and Kelly (2008), photovoltaic modules are connected to charge controllers and DC/CC converters, which allow the batteries to be fully charged and prevent over-

**Table 2.13** Efficiency of silicon-based photovoltaic panels (Reproduced from ANEEL 2011)

Photovoltaic panel type	Efficiency (%)
Monocrystalline silicon	12–14
Concentrated silicon	13–15
Polycrystalline silicon	11–13
Amorphous silicon	3–5

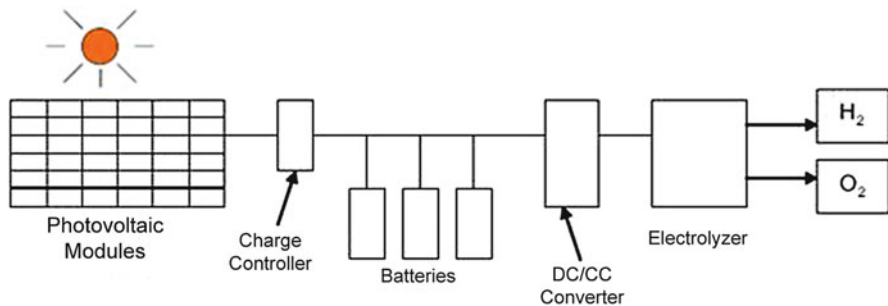


**Fig. 2.29** Conventional solar hydrogen production system (Adapted from Gibson and Kelly 2008)

discharging; these converters are needed to supply the typical voltage characteristic of an electrolyzer. A representation of the system can be seen in Fig. 2.29.

When a photovoltaic panel is connected to any equipment, voltage drops below open-circuit due to the internal resistance of the module and equipment. The DC voltage applied to the electrolysis system is limited by the output of the panel circuit, and the voltage and current of the electrolysis process are limited by the operating characteristics of the electrolyzer, hence the need for a DC/DC converter (Gibson and Kelly 2009).

### 2.7.3 Hydroelectric Generation from Water Spillage

Hydropower is based on obtaining electrical energy through harnessing the hydraulic power of a particular segment of a river through the construction of a dam and, consequently, the creation of a reservoir (Pimentel et al. 2012).

For many years, the Brazilian energy generation park has been fundamentally composed of hydroelectric power plants, where the low cost of this type of energy is associated with abundant natural water catchment areas, which enabled the country to reach a prominent position as one of the world's leading energy producers. The electricity derived from hydroelectric power plants accounts for 67.48 % of the installed generation capacity in Brazil, according to the Brazilian Electricity Regulatory Agency (ANEEL 2014). Hydropower generation projects are divided into three groups: the micro hydroelectric power plants (up to 1 MW of installed generation capacity), the small hydroelectric power plants (between 1.1 MW and 30 MW of installed generation capacity), and large hydroelectric power stations (with over 30 MW). According to the Generation Database of ANEEL (2014), Brazil has 1.108 hydroelectric power plants with installed generation capacity of 86.918 MW.

As these power plants are capable of storing only water and not energy, there are periods when the water surplus has to be released by the spillways and a significant amount of water is spilled yearly, thus ceasing energy production. These waters could be harnessed for generating electricity, so as to feed electrolyzers in order to



produce hydrogen. Hydrogen can be stored, thus harnessing this energy well can increase the energy efficiency of power plants and minimize water spillage, as well as enabling the introduction of a totally clean energy vector into the energy matrix, thus contributing to green energy generation.

The energy generation potential of Itaipu Dam has been the aim of studies of several Brazilian researchers, with respect to harnessing the power of this amount of water spillage. Power plant managers have been discussing the possibility of building an electrolysis plant since 2003, and have already purchased an electrolyzer, although it has not been installed, yet. Figure 2.30 shows a chart with the difference between the average power production and the amount of energy that could have been harnessed, which has not been generated due to water spillage.

According to Fig. 2.30, it is observed that, in all studied years, a considerable amount of energy ceases to be produced. In 2010, the Dam no longer generated an average power production of 1508 MW, the highest amount since 2006.

Dams suffer from a few drawbacks, which contradict the concept of clean and cheap energy generation. Studies show that Balbina, Tucuruí, and Samuel, the three largest hydroelectric power plants operating in the Amazon region, emit pollutants in the same proportion as coal plants. This may come to you as a surprise, but in the first 10 years of operation of a power plant in the Amazon, organic matter rots on account of being covered by water. This is a very strong process of decay, which acidifies the water and releases methane ( $\text{CH}_4$ ) which is 21 times more harmful than carbon dioxide ( $\text{CO}_2$ ) as regards the greenhouse effect (Azenha 2013).

A hydroelectric power plant is aimed at generating electricity by harnessing the hydraulic power of rivers. In this case, electrolysis would only be justified if the electricity generated from the water that would have been spilled were used, i.e.,

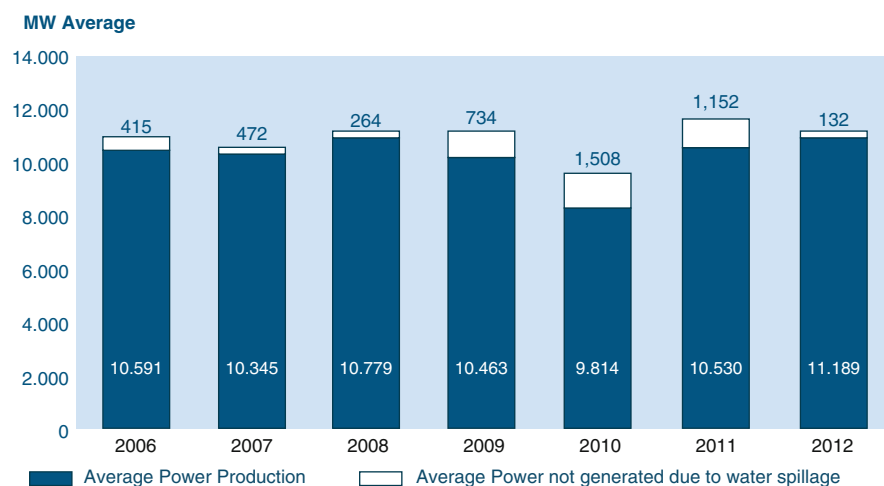


**Fig. 2.30** Average power production and water spillage at Itaipu Dam (Reproduced from ITAIPU 2014)

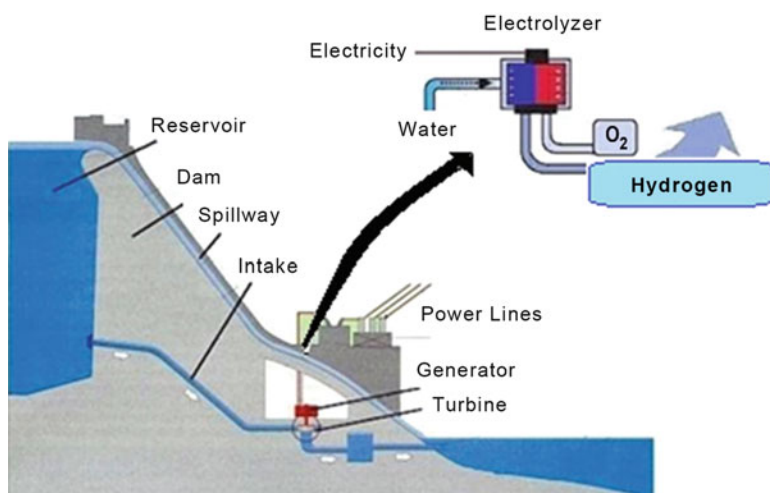


**Fig. 2.31** Electrolysis from water spillage in a hydroelectric power plant

using the surplus energy of the plant for hydrogen production. Figure 2.31 shows a system of hydrogen production by electrolysis using hydraulic energy.

According to Fig. 2.31, the water that would pass through the spillway should have been used to power a generator that would, in turn, supply an electrolyzer with electricity, thus producing hydrogen through water electrolysis.

In the case of Brazil, due to the country's large hydroelectric power generation potential, electrolysis by harnessing the water spilled in hydroelectric power plants can be quite promising. As previously noted in Fig. 2.30, *Itaipu* has enough potential to generate energy from water spillage yearly, which could supply small towns with enough electricity; however, it is not harnessed due to the lack of transmission lines or because there is no demand (FAPESP 2013). By using this energy to power an electrolyzer, hydrogen could be produced, stored, and distributed to these small communities that suffer from the lack of transmission lines.

## 2.8 Biological Hydrogen Production

### 2.8.1 Fermentative Hydrogen Production

Hydrogen production by fermentation of biomass residues is a process with great potential since it has a low environmental impact and is of simple implementation, in other words, it is relatively low price and ease of building a facility to process the residues and obtain hydrogen when compared to other processes. It is also important to note a few other advantages of production by this process, such as local

integration due to the possibility of adapting to the use of different types of raw material, use of the fermentation residues as fertilizer, and also reducing the economic and environmental impact of fuel transportation (Foglia et al. 2011; Claassen and de Vrije 2006).

The anaerobic fermentation usually takes place in four steps: hydrolysis, acidogenesis, acetogenesis, and methanogenesis.

- Hydrolysis: The first stage of fermentation, where the particulate matter is dissolved, thus being able to cross the cell walls of the bacteria responsible for fermentation. This is due to the excretion of exoenzymes by the bacteria.
- Acidogenesis: The process takes place after the hydrolysis, breaking the molecules into smaller ones inside the cell. As a result of the acidogenesis process, the formation of volatile fatty acids, carbon dioxide production, ammonia, and hydrogen sulfide occurs.
- Acetogenesis: In this stage of the process, the previous stage products are oxidized. They are digested, forming hydrogen, acetic acid, and carbon dioxide.
- Methanogenesis: This is the final stage of the anaerobic digestion process, with the formation of methane, water, and carbon dioxide.

The fermentation process is shown in Fig. 2.32 below:

Some factors interfere with the fermentation process. Among which are the influence of temperature, raw material composition, particle size, pH, among others.

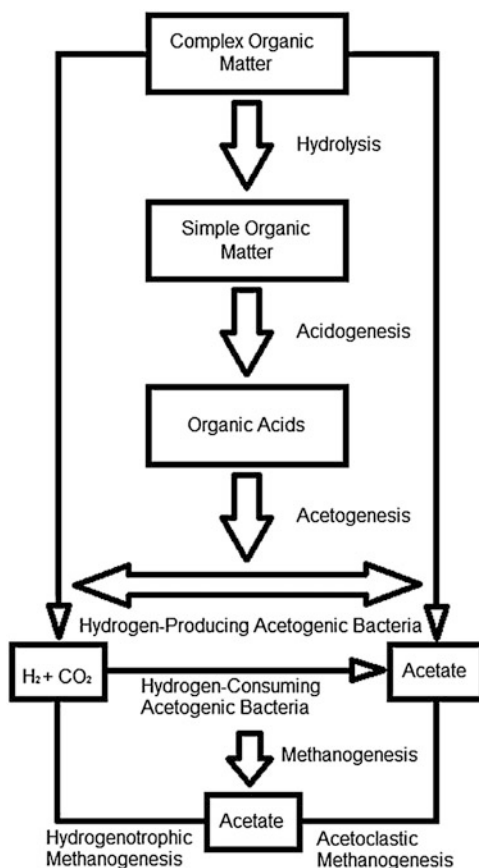
There are several materials that can be used as feedstock for hydrogen production by fermentation. The most commonly used ones are rich in lipids, proteins, and carbohydrates, the latter being the preferred source for the fermentation process.

### 2.8.2 Enzymatic Hydrogen Generation

According to Woodward et al. (2000a, b), marine thermophilic anaerobes are able to produce hydrogen and carbon dioxide. For such a purpose, the hydrogenase from *Pyrococcus furiosus* should be coupled in vitro with glucose dehydrogenase in order to produce one mole of hydrogen per mole of glucose (Woodward et al. 1996; Inoue et al. 1999). Since the same NADP<sup>+</sup> cofactor, i.e., nicotinamide adenine dinucleotide phosphate (Ma et al. 1993, 1994), was selected to be used for both enzymes, it is recycled while the glucose substrate is being oxidized for molecular hydrogen production. This system can also be used to produce hydrogen from sucrose or cellulose. Thus, appropriate enzymes such as invertase or cellulase must be added (Woodward and Orr 1998; Woodward et al. 2000a, b).

The anabolic pentose phosphate pathway (PPP) is commonly found in most organisms. Its oxidative branch comprises two enzymes: glucose 6-phosphate dehydrogenase and 6-phosphogluconate dehydrogenase. Such enzymes together produce 2 mol of NADPH and 2 mol of ribose 5-phosphate from one mole of glucose-6-phosphate. The non-oxidative branch makes one and two carbon

**Fig. 2.32** The anaerobic digestion process (Adapted from Santos 2004)



transfers, which convert pentoses into fructose 6-phosphate and glyceraldehyde 3-phosphate. Given that fructose 6-phosphate can be isomerized into glucose 6-phosphate through phosphohexose isomerase (glucose 6-phosphate isomerase), they can be recycled back into NADPH for further hydrogen production. The addition of hydrogenase theoretically obtains 12 H<sub>2</sub> mol per 1 mol glucose 6-phosphate. A yield close to the aforementioned theoretical value (11.6 mol H<sub>2</sub> per 1 mol glucose 6-phosphate) was reached by combining PPP mesophilic PPP enzymes and *P. furiosus* hydrogenase, which is depicted in Fig. 2.33 (Woodward et al. 2000a, b).

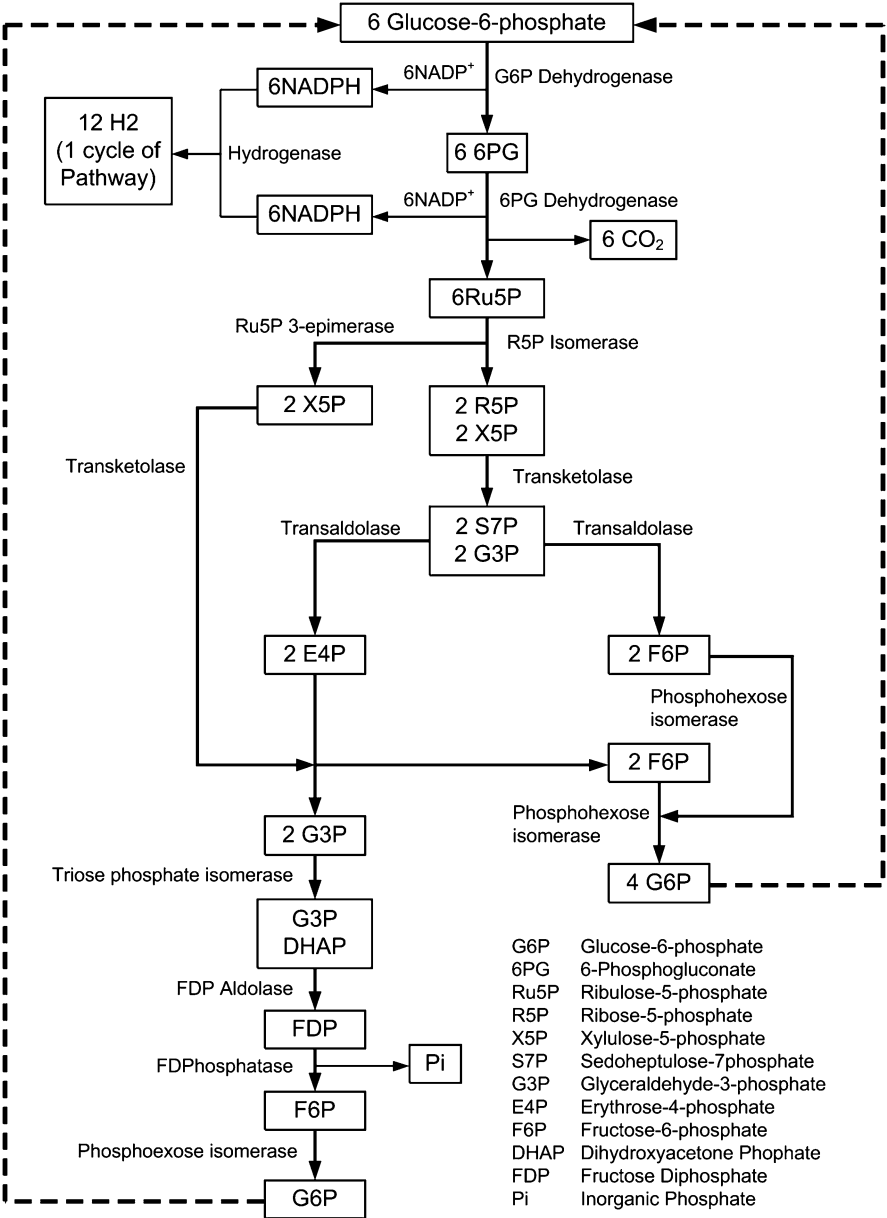


**Fig. 2.33** Hydrogenase and enzymes of the PPP for hydrogen production (Adapted from Woodward et al. 2000a, b)

### 2.8.3 *Biocatalyzed Electrolysis*

According to Rozendal (2007), biocatalyzed electrolysis is a feasible hydrogen production method, since it is:

- Capable of converting dissolved organic compounds
- Able to deal with the endothermic nature of the conversion reactions of many dissolved organic compounds into hydrogen in a more practical way than using sunlight
- Robust and flexible, as it will be designed for hydrogen production from wastewater
- Based on mesophilic mixed cultures that grow along the process through natural selection
- Able to convert a wide range of organic substrates

A biocatalyzed electrolysis system makes use of electrochemically active microorganisms which are able to transfer electrons from the inner to the outer part of the cell and capable of growing on the surface of the electrode during its use as electron receiver for the oxidation of organic compounds in which it is immersed. Since electrochemically microorganisms release electrons at a high energy level while immersed, a low potential will appear on the electrode, thus producing hydrogen (Rozendal 2007).

The schematic model of a fuel cell based on this principle is shown in Fig. 2.34.

### 2.8.4 *Hydrogen Production from Algae (Photobiological Water Splitting)*

Algae are amongst the most resistant organisms on the planet, which are able to grow in diverse conditions. They are typically found in damp places or bodies of water (fresh and seawater) and are, therefore, common in terrestrial and aquatic environments. They do not have the various structures that characterize terrestrial plants, such as leaves and roots, and are different from other microorganisms due to the presence of chlorophyll. They possess photosynthetic capacity in a single cell, thus facilitating genetic and metabolic research conduction in a much shorter period of time than in the case of conventional plants. The major components of green algae are: clearly defined nucleus, cell wall, chloroplasts containing chlorophyll and other pigments, pyrenoid, stigma, and flagella (Pelczar et al. 2008).

Biological hydrogen production from algae has been considered as being sustainable and advantageous in comparison with thermochemical and/or electrochemical processes, due to the purity of hydrogen (over 98 %), use of a simple solar reactor, and the consumption of CO<sub>2</sub> during their growth phase; moreover, they are capable of fixing CO<sub>2</sub> more efficiently than terrestrial plants (in about ten times) as regards the amount of biomass per m<sup>2</sup> (Usui and Ikenouchi 1997).

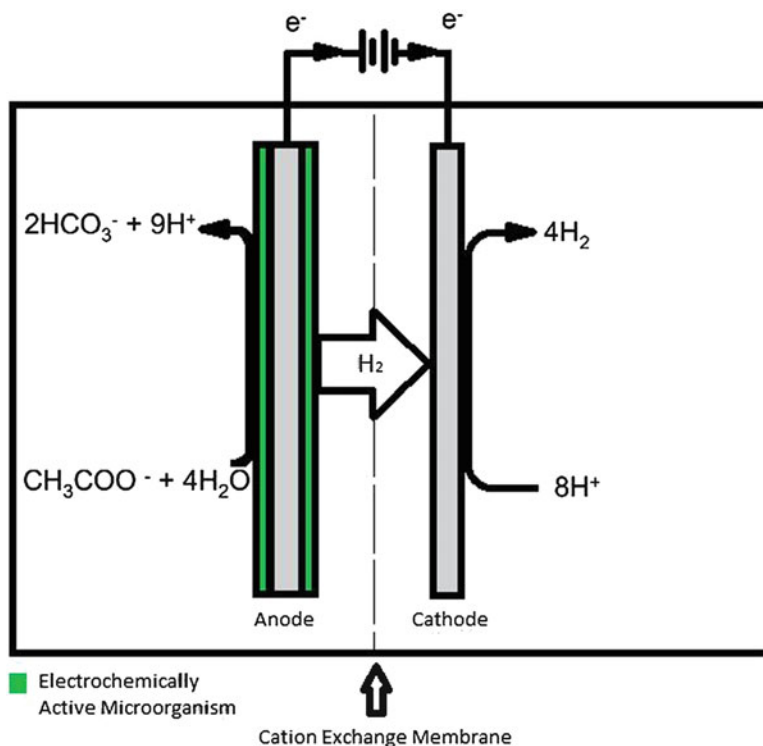


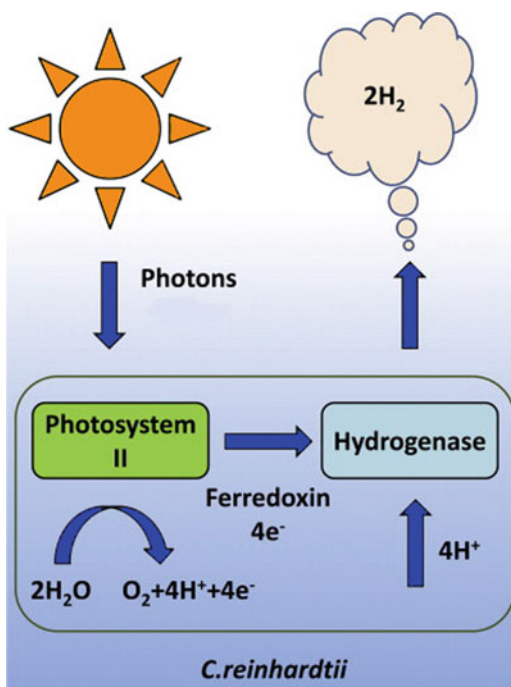
**Fig. 2.34** Microbial fuel cell (Adapted from Logan et al. 2006)

In comparison with different types of algae for hydrogen production, the microalgal strain *Chlamydomonas reinhardtii* (*C. reinhardtii*) presents one of the simplest lifecycles, of easy manipulation with rapid growth, and one of the best hydrogen production rates (Hemschemeier 2005; Ministry of Agriculture and Agroenergy 2006). Hydrogen production from this strain is usually performed by direct biophotolysis, as shown in Fig. 2.35 (Ahmed et al. 2011; Hallenbeck and Benemann 2010; Das and Veziroglu 2008).

Direct biophotolysis occurs in the presence of light and under anaerobic conditions. According to Fig 2.35, in photosystem 2 (PS II), light energy is captured by pigments. These pigments are usually chlorophyll and carotenoids attached to proteins to form a complex which absorbs photons. This absorbed energy is transferred to the reactive core of this photosystem, and the energized electrons are transferred by the ferredoxin to the hydrogenase. To replace these lost electrons, the reactive core withdraws electrons from two water molecules, resulting in the detachment of  $\text{O}_2$  and release of four hydrogen ions ( $4\text{H}^+$ ) (Lehninger et al. 2010).

Hydrogenase is activated only under anaerobic conditions, and it uses the electrons received by ferredoxin to reduce protons ( $\text{H}^+$ ) to hydrogen molecules ( $\text{H}_2$ ) (Lehninger et al. 2010).

**Fig. 2.35** Hydrogen production by direct biophotolysis from *C. reinhardtii* (Adapted from Tamburic et al. 2011)



After years of research, it was observed that in closed cultures, the deprivation of sulfur in these organism strains results in oxygen consumption and anaerobiosis in the culture medium. Thus, the medium microorganisms are performing an alternative photosynthesis, which uses light and hydrogenase for  $\text{H}_2$  production (Tao et al. 2008).

#### 2.8.4.1 Hydrogen Production Process from the Strain *Chlamydomonas reinhardtii*

The experimental photobiological hydrogen production from green microalgae *C. reinhardtii* occurs in two steps. The first one refers to culture the algae and the second one to hydrogen production. Thus, it occurs in two different reactors, as shown in Fig. 2.36.

In the first reactor, the algae grow in the presence of light, with normal concentration of sulfur, where pH and temperature should remain close to 7 and 25 °C, respectively (Effendi et al. 2005; Haag et al. 2007). The specific composition of the medium for the growth of this microalgal strain is presented in Table 2.14.

At room temperature and pressure of 1 atm (Levin et al. 2004), the content of the first reactor is transferred to the second reactor after being centrifuged or diluted (10 % v/v), which contains a medium without sulfur and whose composition is



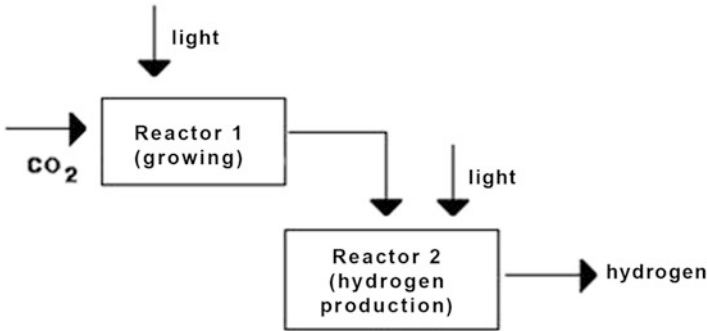


Fig. 2.36 Hydrogen production from green microalgae

**Table 2.14** Composition of the *C. reinhardtii* growth medium: Tris-acetate-phosphate (TAP) (Adapted from Xu et al. 2004)

Medium prior to TAP		TAP	
15 g	NH <sub>4</sub> Cl	25 mL	Medium prior to TAP
4 g	MgSO <sub>4</sub> ·H <sub>2</sub> O	0.375 mL	Phosphate solution
2 g	CaCl <sub>2</sub> ·H <sub>2</sub> O	1 mL	Trace elements (EDTA, Zn, B, Mn, Co, Cu, Mo and Fe salts)
Dissolve in 1 L of water		1 mL	Acetic acid
		2.42 g	Tris-aminomethane
		Dissolve in 1 L of water	

**Table 2.15** Hydrogen production medium composition without sulfur (TAP-S) (Adapted from Xu et al. 2004)

Medium prior to TAP-S		TAP-S	
15 g	NH <sub>4</sub> Cl	25 mL	Medium prior to TAP-S
4 g	MgSO <sub>4</sub> ·H <sub>2</sub> O	0.375 mL	Phosphate solution
2 g	CaCl <sub>2</sub> ·H <sub>2</sub> O	1 mL	Trace elements (sulfur salts replaced by chloride salts)
Dissolve in 1 L of water		1 mL	Acetic acid
		2.42 g	Tris-aminomethane
		Dissolve in 1 L of water	

presented in Table 2.15. The media of the first and second reactor are known as TAP and TAP-S, respectively.

In Tables 2.14 and 2.15, it is observed practically the same composition for both media, and the only difference is in the absence of sulfur in the TAP-S medium. Thus, sulfur salts are replaced by chloride salts. For the purpose of media formation, a TAP or TAP-S solution is firstly made. After this step, 25 mL of this solution, 0.375 mL of the phosphate solution, 1 mL of trace elements, 1 mL of acetic acid, and 2.43 g of Tris-aminomethane are dissolved in 1 L of water, thus obtaining the media for algae growth (TAP) and hydrogen production (TAP-S).

### 2.8.5 *Photobioreactors for Hydrogen Production from Algae*

Microalgae can be cultured through open systems (ponds) or in closed systems, called photobioreactors (PBR).

#### 2.8.5.1 Open Systems

The greatest advantage of open systems is its simplicity, which results in low production and operation costs (Singh and Sharma 2012). The tanks are usually called raceway ponds (Fig. 2.37) which are filled with natural waters, made of concrete or simply dug into the ground and coated with plastic to prevent the soil from absorbing the liquid, and their depth is limited so that the algae can be exposed to sunlight. Although this method is the simplest of all cultivation techniques, it presents some drawbacks: out-of-control condition, being highly vulnerable to contamination by other microorganisms and lower biomass productivity.

Generally speaking, the productivity of these systems is  $0.5 \text{ g L}^{-1}\text{d}^{-1}$ , well below the levels reached by photobioreactors because high cellular density cannot be attained. An average depth of 20 cm results in insufficient agitation, as well as leading to low rates of gas-liquid mass transfer and an increase in residence time of the culture at the bottom of the pond (dark zone). In order to overcome the problems associated with an open system, researchers usually select closed systems of monocultures (Singh and Sharma 2012).



**Fig. 2.37** Open system for algae cultivation (raceway ponds) (Reproduced from the Sahara Forest Project 2013)

### 2.8.5.2 Photobioreactors

Photobioreactors are closed culture systems, which are mainly applied in the controlled production of biomass and hydrogen production processes. Despite their elevated costs and design limitations, their mass transfer rate, due to the tendency to accumulate  $O_2$ , offer several advantages over open systems (Singh and Sharma 2012), which are:

- Minimizing contamination
- Offering better control of conditions, such as pH, temperature, light, and  $CO_2$  concentration
- Avoiding water evaporation
- Favoring cell concentration

There are several types of photobioreactors, but the most commonly used ones are the tubular and plate photobioreactors. These are systems aerated by gas injection and usually have an agitation mechanism. They can be aligned horizontally, vertically, or inclined, as shown in Fig. 2.38.

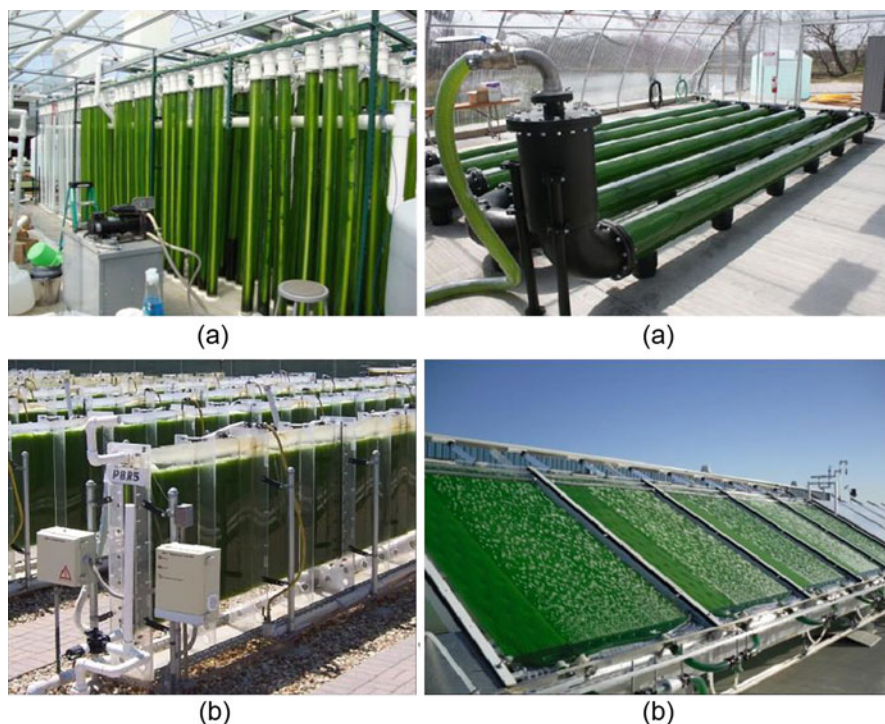


**Fig. 2.38** Tubular (a) and plate photobioreactors (b) (Reproduced from Kwietniewska et al. 2012; University of Nevada 2013; Arizona State University 2013; Energy Options 2013)

According to Burgess et al. (2011), plate photobioreactors are between 1 and 5 cm thick, and their height and length may vary. They have high surface-area-to-volume ratio and, therefore, achieve high energy efficiency when compared to tubular photobioreactors (Cortés 2009). Tubular photobioreactors have a maximum diameter of 10 cm, and also present a large illuminated area. Their main disadvantage is the gradient difference in pH, O<sub>2</sub>, and CO<sub>2</sub> dissolved along the pipeline.

All closed systems present advantages and disadvantages, therefore, choosing the type of photobioreactor depends on the process, product to be obtained, species involved, economic assessment, and installation region, as well (Sugai 2012).

## 2.9 Other Hydrogen Production Processes

### 2.9.1 Gasification

#### 2.9.1.1 Gasification Theory

Biomass gasification technologies have been used since 1800s (Reed and Das 1998), and the first application occurred in gas production from coal. Since the 20s, gasification has been used to produce synthetic chemicals. The most commonly known technique is the Fischer-Tropsch process for the production of liquid hydrocarbons from synthesis gas. Currently, some gasifiers using coal as fuel are still in operation, but the number of gasifiers fueled by biomass is still limited.

The gasification technology for obtaining liquid and gaseous fuels from biomass as raw material has gained new impetus, since it represents a breakthrough for producing a sustainable alternative of energy carriers (Van der Meijden 2010).

The term gasification is applied to processes that aim at transferring the energy contained in solid or liquid fuels to a gaseous energy carrier with minimal energy loss. The producer gas has a lower heating value (LHV) of around 4–7 MJ/Nm<sup>3</sup> (if the gasifying agent is air), or from 10 to 18 MJ/Nm<sup>3</sup> (if the gasifying agent is oxygen or steam). The heat required for the process can be supplied by burning part of the fuel (gasification) or from an external source (indirect gasification) (Sánchez et al. 2008).

The syngas can have different applications, depending on its quality: for starting internal combustion engines, gas turbines, direct burning, and synthesizing chemical components (Andrade 2007). General specifications that the gas must meet so that it can be applied in modern engines were standardized in the late 1980s, and are reported in Table 2.16 (Van de Beld 2001).

**Table 2.16** Gas specifications for internal combustion engine use (Adapted from Van de Beld 2001)

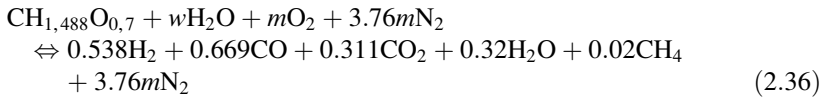
Parameters	Unit	Acceptable	Great
Gas LHV	kJ/Nm <sup>3</sup>	>2500	>4200
Particulate matter content	mg/Nm <sup>3</sup>	<50	<5
Particle size	μm	<10	<1.0
Tar content	mg/Nm <sup>3</sup>	<500	<100
Acetic acid	ppm	<50	0
Hydrochloric acid	ppm	<500	0

### 2.9.1.2 Gasification Zones and Main Reactions

Gasification is the conversion of solid biomass into a gas fuel (and a portion of sensitive heat), whereas in combustion, the heat capacity of the solid is completely transformed into sensitive heat. Gasification provides some advantages when compared to direct combustion, such as the resulting gas presents better combustion properties than solids, its combustion process is simpler to manage and requires a smaller amount of air with no particulate emissions, thus resulting in less air pollution and better management of the plant.

The chemical composition of bagasse, once it is dry, can be regarded as being approximately constant and equal to  $\text{CH}_{1,488}\text{O}_{0,7}$ .

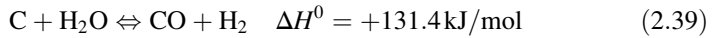
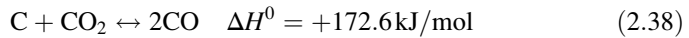
The overall reaction of the gasification of bagasse with air can be schematically described by Eq. (2.36) (Pérez et al. 2014):



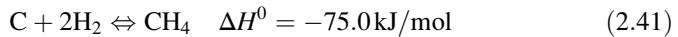
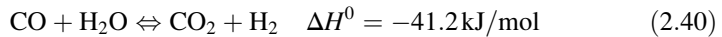
After the biomass dehydration and pyrolysis process, the products react with oxygen in a temperature ranging from 1000 to 1200 K (Reed and Das 1998). Initially, the combustion reaction occurs as follows:



Afterwards, a chain of reactions occur, where the main ones are the Boudouard reaction of carbon conversion with  $\text{CO}_2$  and steam.

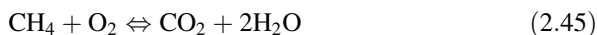


These reactions occur slowly, thus controlling the speed of the gasification process. The successive reactions are:



In the first one, hydrogen is produced by the water-gas shift reaction, and methane production occurs on the next one. In the gasification zone, the following secondary reactions occur:





The kinetics of these reactions is difficult to be determined in the actual conditions of gasification because the process is usually studied as a whole.

It is clarified that this theory is not always valid for all types of gasifiers, thence it is necessary to consider that the residence time of all species should be sufficient to reach a state of thermodynamic equilibrium in the system. Ideally, there should be a complete conversion of biomass, but, in fact, it does not happen.

The obtained product typically contains a variable amount of tar and hydrocarbons. The gasification occurs at high temperatures, where there are only a few stable combinations of produced elements, which are: CO, CO<sub>2</sub>, CH<sub>4</sub>, H<sub>2</sub>, H<sub>2</sub>O, and a few hydrocarbons (C<sub>x</sub>H<sub>y</sub>).

The gas produced in the gasification process also contains tar. Tars are heavy hydrocarbons, which can cause incrustation problems when the gas is cooled; it can also contain other pollutants, such as H<sub>2</sub>S, thiophene, NH<sub>3</sub>, HCl, HCN, COS (Carbonyl sulfide), and solid particles, that have to be removed before the gas is used in some applications (Van der Meijden 2010).

A widely used approach consists in expressing the concentration of different species as a function of temperature and consumed oxygen; the latter is represented by the equivalence ratio (ER) (Reed and Das 1998):

$$\text{ER} = \frac{\text{oxidizer mass/dry fuel mass}}{\text{oxidizer mass /fuel mass}^*} \quad (2.46)$$

\*mass stoichiometric ratio for complete combustion.

This parameter, arbitrarily introduced along with temperature, efficiently describes the gasification process. When  $0 \leq \text{ER} \leq 0.2$ , pyrolysis occurs with an oxygen deficit; however, if  $\text{ER} \geq 1$ , a complete combustion occurs, with a theoretical or higher amount of air. As for the gasification process, the ER generally varies between 0.2 and 0.4 (Reed and Das 1998). Table 2.17 shows the stoichiometric air calculation for the combustion of 1 kg of bagasse with the composition considered in this study.

### 2.9.1.3 Types of Gasifiers and Main Operation Feature

The characterization of gasifiers can be made according to different properties, such as bed temperature and type, relation between the gasifying agent and fuel, pressure and ash formation. As regards temperature conditions, reactors can be classified into high-temperature gasifiers (typically from 1500 to 1800 K) which produce a gas with higher heating values (10–18 MJ/Nm<sup>3</sup>) (*syngas*) and average-temperature gasifiers (typically 1123 K) which produce a fuel gas with lower heating values (4–7 MJ/Nm<sup>3</sup>). The *syngas* contains low hydrocarbon content as methane, but the

**Table 2.17** Stoichiometric air determination according to the aforementioned bagasse composition

Component	[kg/100 kg of bagasse]	Molar mass component [kg/kmol]	Component substance quantity [kmol]	Product	[kmol O / kmol component]
C	36.56	12	3.05	CO <sub>2</sub>	6.09
H	4.37	1	4.37	H <sub>2</sub> O	2.19
S	0	32	0.00	SO <sub>2</sub>	0.00
O	31.25	16	1.95	–	–1.95
N	0.16	14	0.01	N <sub>2</sub>	0.00
W	25	18	1.39		0.00
O stoichiometric moles (kmol)/100 kg solid					6.33
O <sub>2</sub> stoichiometric moles (kmol)/100 kg solid					3.16
Oxygen volume per kg of solid Nm <sup>3</sup> /kg solid					0.71
Oxygen mass per kg of solid (kgO <sub>2</sub> /kg solid)					1.01
Considering air composition with 21 % oxygen					
Required air (kmol)/100 kg solid					15.07
Air volume per kg of solid (Nm <sup>3</sup> Ar/kg solid)					3.37
Air mass per kg of solid (kg Ar/kg solid)					4.36

gas from average-temperature gasifiers contains high hydrocarbon content (primarily CH<sub>4</sub>, C<sub>2</sub>H<sub>4</sub>, and C<sub>6</sub>H<sub>6</sub>), depending on the type of reactor, biomass, and gasification agent being used (Sánchez et al. 2008).

The most efficient type for syngas production is the entrained-flow gasifier. Such gasifiers, which operate on coal and technologies developed by Shell, General Electric and Siemens, are commercially available in the order of tens and hundreds of thermal megawatts. They are mainly operated at high pressure conditions (typically from 3000 kPa) to maximize the efficiency of the process in the reactor. Typically, O<sub>2</sub> (diluted with steam) is used as gasification agent. The gasifier always works above the ash fusion temperature in order to keep it in its liquid form. The syngas produced by the gasifier is subsequently cooled so as to solidify the gas along its purification process (Vreugdenhil et al. 2009).

Average-temperature gasifiers can be classified based on their bed, such as fixed-bed and fluidized bed gasifiers. Fixed bed gasifiers can be classified into co-current gasifiers (*Downdraft*) and counter-current gasifiers (*Updraft*). Both are commonly used for biomass gasification. Figure 2.39 shows the basic principles of a typical operation of updraft (a) and (b) downdraft gasifiers.

Downward gasifiers are widely used for small-scale cogeneration. Their typical input thermal powers are between 100 and 1000 kW. The fuel is biomass with moisture content of around 20 %. The advantage of this technology is that the produced gas contains low tar and particulate matter content, and its technology is relatively simple.

A fixed-bed gasifier also requires a uniform fuel distribution for a continuous and reliable operation. The carbon content of ashes at the bottom of gasifiers is usually high (>10 wt%) because the fuel conversion is not complete along the gasification process. The downdraft technology is not suitable for being applied on an industrial



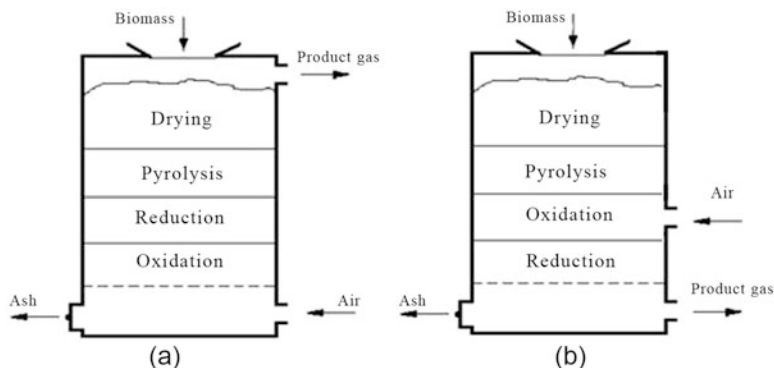


**Fig. 2.39** Fixed-bed gasifiers operation: (a) updraft and (b) downdraft

scale because, among other reasons, it requires an increase in bed diameter; such an increase raises the risk of channeling, thus producing a homogeneous distribution of oxygen in the gasification section and decreasing the efficiency of the process.

Updraft gasifiers are more suitable for being applied on an industrial scale and are less sensitive to variation in moisture content and biomass shape, but produce a large amount of tar in their traditional design. If tar were completely removed, the gas could be combusted in a gasoline engine. Tar is normally removed once it is combined with water, and this water flow requires a thorough purification process before being released into a sewer system. The overall efficiency of the updraft reactor can be increased due to a high rate of carbon and gas conversion, moreover, because the syngas is released at a low temperature from the gasifier. The tar removal and water cleaning make the process complex and too expensive for being applied on a small scale (<1 thermal MW). An example of a successful updraft reactor can be found in a plant called Harboøre in Denmark (Paisley et al. 1991; Van der Meijden 2010).

Fixed-bed biomass gasifiers (updraft and downdraft) are operated in dry mode, which means that ashes do not reach their melting point. This result is achieved by keeping the operating temperature of the reactors below the melting point of ashes. Both types of gasifiers generally use air as gasifying agent. Fixed-bed gasifiers are not seen as an option for producing synthesis gas from biomass because of their inability to produce a nitrogen-free gas when using air as gasifying agent, in addition to the amount of tar in the fuel gas.

#### 2.9.1.4 Gasification in Fluidized Bed Theory

Fluidized bed gasifiers can be operated in such a way as to produce a gas which is either nitrogen-free or low in nitrogen. The technology is suitable to be expanded to several tens of MW. These gasifiers have been widely used for several years, and their advantages over fixed-bed gasifiers lie in the uniform temperature that is



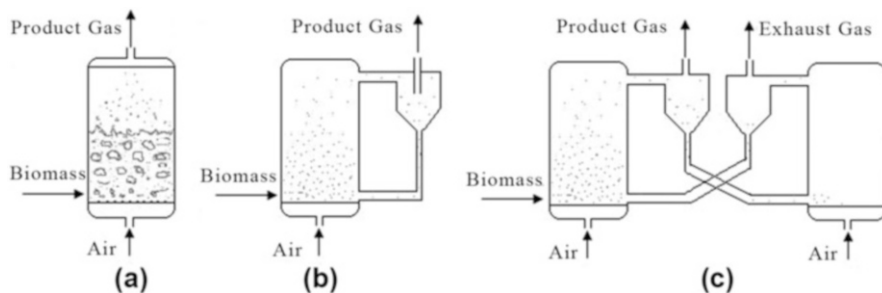


**Fig. 2.40** Fluidized bed gasifiers: (a) bubbling fluidized bed, (b) circulating fluidized bed and (c) indirect gasification

reached in the gasification section and the greater speed of the gasification reaction occurrence (Raj and Goic 2011).

Fluidized bed reactors are those in which the gasifying agent circulates through its interior at such a rate that the bed is found in a fluidization state, where there are various conditions that intensify the energy and material transfer between the fuel and the gas. In this type of system, the gasifying agent enters through the bed of particles at a rate which is enough to keep them suspended. The bed is heated and, when high temperatures are reached, the fuel particles are introduced, reaching bed temperature quickly. Biomass gasification in fluidized-bed reactors requires, in general, small fuel particles ( $<6$  mm) and a moisture content which is preferably less than 30 % of its weight (Basu 2006).

Fluidized bed gasifiers can be divided into three main categories: bubbling fluidized bed (BFB), circulating fluidized bed (CFB), and indirect gasification with dual fluidized bed. All fluidized bed gasifiers use an inert material in their bed, which can be ordinary sand, fuel ashes, or a catalytically active bed material, such as dolomite or olivine. The purpose of the bed material is to conduct and distribute heat through the gasifier, so as to homogenize the temperature, mix the fuel with the gasifying agent and the syngas, and, in the case of a catalytically active material, reduce the concentration of tar. Figure 2.40 shows the basic principles of the three types of fluidized bed gasifiers (CIRCE 2005; Van der Meijden 2010).

In a bubbling fluidized bed gasifier (BFB), the fuel is usually fed at the base of the bed. The bed material is fluidized by a gasifying agent (air, oxygen, or a mixture of steam and oxygen) that enters the gasifier by means of injectors distributed at the bottom of the reactor. In such reactors, the fluidization speed of the gasifying agent is low because there is a significant movement of the solid; the gasifying agent's typical speed is 1 m/s. Oxygen is used in the bed for combusting part of the gas and/or coal to produce the necessary heat for triggering the typical thermochemical reactions of the process. These gasifiers are usually applied on a scale of less than 10 MW (thermal gasifiers). The reason for this capacity limitation is that there must be a good distribution of the fuel along the bed, which becomes more difficult as the reactor diameter increases. Table 2.18 presents a comparison between the circulating and bubbling fluidized bed gasifiers (Williams 1996).

**Table 2.18** Comparison between circulating and bubbling fluidized bed reactors (Adapted from Williams 1996)

Fluidized bed reactor	Temperature [K]		Biomass	Feed	Gasifying agent	Tar content
	Reaction	Outlet				
Bubbling (BFB)	973–1273	973–1073	Wood chips, corn cobs, rice husk	Directly into the bed area	Lower part of the gasifier	Relatively high
Circulating (CFB)	973–1273	873–1073	Bagasse, wood chips, rice husk, sawdust	Directly into the bed area	Lower part of the gasifier	Low

Circulating fluidized bed gasifiers (CFB) have higher fluidization speeds and, for this reason, the bed material is dragged, thus requiring circulation to maximize fuel conversion. The speed of a typical gasifying agent is usually between 3 and 10 m/s, which is much higher than in the case of BFB. The dragged bed material and the fuel particles that have not been converted completely are removed from the gas through a cyclone separator or another device. The particles will typically return to the bottom of the gasifier through a nonmechanical valve. Such nonmechanical valve can be a tube that also has the function of preventing gas leaks at the bottom of the solid outlet in the cyclone separator. The company Foster Wheeler successfully implemented this type of gasifier on a commercial scale in a project developed in Lahti, in Finland, and in Ruien, Belgium (Paisley et al. 1991; Van der Meijden 2010).

On indirect gasification, the biomass gasification separation and the remaining coal is combusted in separate reactors, as shown in Fig 2.40c. The biomass fed into the first reactor is converted into gas and coal. The heat required for the process is conducted through the circulating bed material, and it is originated from the second combustion reactor. The coal and the bed material are separated from the gas by a separating device (for example, a cyclone separator); the syngas leaves the gasifier and goes through a purification process.

### 2.9.1.5 Advantages of Fluidized Bed Gasification

The main advantages of fluidized bed reactors include: better control of temperature and reaction rates, high specific capacity, potential for dimensioning to magnitudes on the order of hundreds of megawatts, easy adaptation to changes in biomass, and low efficiency losses caused by particles that may not react. These types of reactors also present low sensitivity to variations in fuel moisture (Zainal 2010).

### 2.9.1.6 Disadvantages of Fluidized Bed Gasification

The main disadvantages of fluidized bed gasifiers are particle losses which lead to a decrease in the process efficiency. In addition, the internal walls of the reactor and the elements involved in it cause wear from the high relative speed of the fluid

and friction with the sand and particles. Furthermore, these reactors show moderate and high levels of tar and particles in the exhaust gases and, therefore, require a complex system of gas cleaning and residual water treatment. Another drawback is that the carbon conversion rate is lower than that of fixed bed gasifiers (Zainal 2010).

### 2.9.1.7 Gasification Theory on Entrained Flow

In entrained flow systems, the fuel can be injected along with oxygen, a mixture of steam and oxygen, or air. There is an area where most of the molten slag is collected. The output products that reach high temperatures require prior cooling before the fuel gas goes through its cleaning process, thus resulting in a decrease in the system's thermal efficiency. This gasification technology produces little methane, uses a relatively compact equipment, and involves short reaction times due to high operating temperatures (1300–1800 K) (Larson et al. 2001). During the past decade, Texaco was the most widespread commercial application system of entrained bed gasification to produce synthesis gas. In addition to Texaco's Gasifier, other technologies, such as Shell's and Destec's, were initially developed on a commercial scale in the United States. Although these processes, generally speaking, have lower thermal efficiency than fixed-bed and fluidized bed systems, its resulting gas presents low tar, hydrocarbons that are heavier than methane and nitrogen compound concentrations. Shell, Destec, and Texaco processes can produce up to 2000 t/day (Sánchez et al. 2008).

On account of their proven performance, entrained bed gasifiers have been selected for demonstrations in BIG-GTCC systems in the United States and in a few European countries using coal as fuel. Among such reactors, the following can be described (Sánchez et al. 2008):

- Koppers-Totzek gasifier: Commercially, this is the most important entrained bed reactor in operation.

Figure 2.41 illustrates a Koppers-Totzek reactor. It works at atmospheric pressure and at higher temperatures than other gasifiers. There are two versions: two- and four-headed ones.

The first version of this reactor was developed in the 1951, which works horizontally and has an elliptical shape, while the second one was built in 1970 in India, showing improved performance. Each head contains two burners, and the reactor is coated with a water jacket and refractory material. The molten ashes are removed through the center of the gasifier.

- Texaco Gasifier: It was developed in the United States and consists of a pressurized vertical cylinder covered with a refractory material, which preferably operates with residual bituminous coals mixed with water. Figure 2.42 shows the process flow chart of this type of reactor. In commercial applications, this

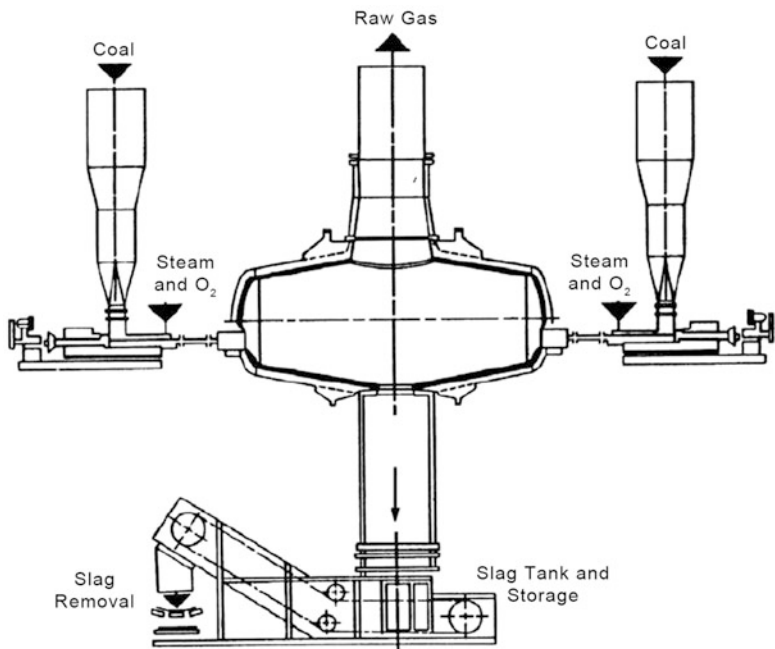


Fig. 2.41 Koppers-Totzek Gasifier (Adapted from Sánchez et al. 2008)

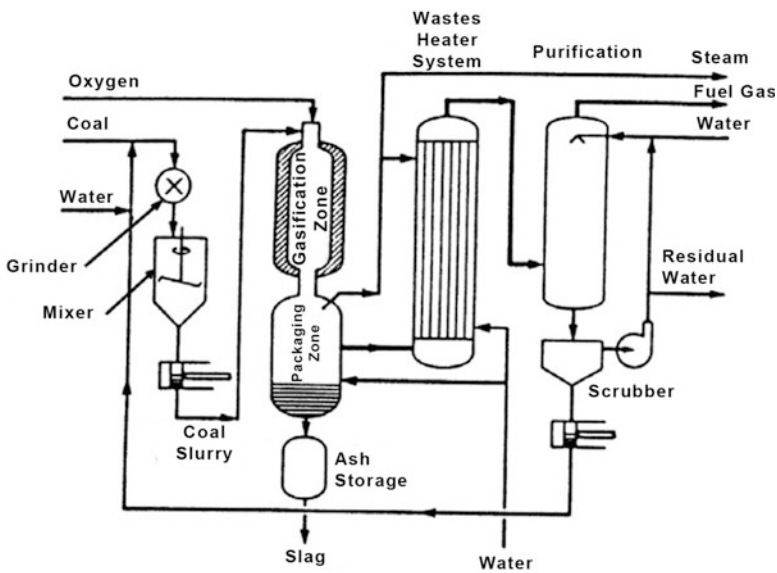
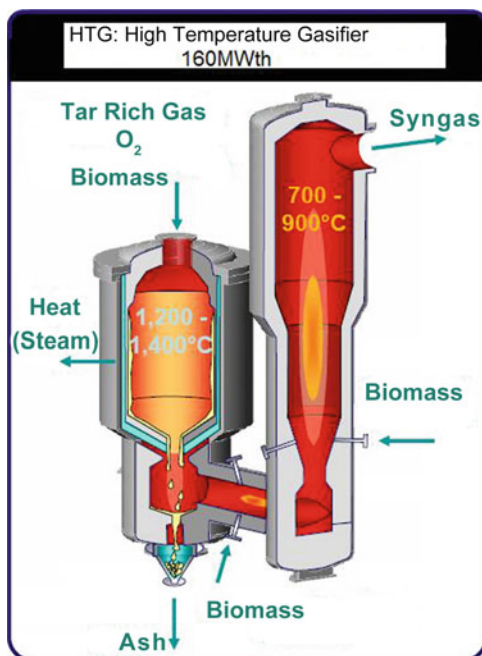


Fig. 2.42 Texaco gasifier process flow chart (Adapted from Sánchez et al. 2008)

**Fig. 2.43** Entrained flow gasifier. CHOREN Technology (Adapted from Worley and Yale 2012)



gasifier produces syngas to produce methanol and acetic anhydride. In California (USA), there is a plant with enough capacity to process 910 t/day of fuel.

- Otto-Rummel Gasifier: This equipment also works at atmospheric pressure and is divided into three stages. In the first stage, the coal is dried and pulverized, which is then injected along with steam and oxygen. In the second stage, the gasification reactions occur and, in the final stage, the resulting gas is collected and cooled. A reactor of this type with 1.8 m in diameter was installed on a commercial scale in 1960 in Germany, which operated steadily for 18 months.
- Shell-Koppers Gasifier: This reactor is a pressurized version of the Koppers-Totzek gasifier with very similar design, but with higher thermal efficiency. There are currently two plants with a capacity of 1000 t/day, one being in Germany and the other one in the Netherlands.
- CHOREN Gasifier: This gasification technology was developed by CHOREN Industries GmbH, one of the most efficient, reaching 81 % efficiency in cold gas (Worley and Yale 2012). The main fuel requirements of such technology are small ones (preferably <6 mm) and with low moisture content (Fig. 2.43).

### 2.9.1.8 Entrained Flow Gasification Advantages

- High quality of resulting gas: it has low tar and methane contents, due to high operating temperatures (above 1300 °C) and to high levels of CO and H<sub>2</sub>

- Capacity to operate with liquid flows or particulate matters of low particle size (bio-oil and torrefied and ground biomass)
- High pressure and power
- Capacity to remove molten ashes

Taking into account the complexity of the physical properties of sugar cane bagasse and the difficulties described in previous attempts of gasifying this fuel in fluidized bed reactors, it was considered the possibility of gasifying the bagasse in a CHOREN entrained bed gasifier after being pretreated, by using a conditioning technique that allows adapting the physical properties of bagasse to those required by this type of gasifier.

## ***2.9.2 Some Considerations About Ammonia Cracking***

### **2.9.2.1 Ammonia Cracking**

The use of ammonia as chemical compound (medium) for storing hydrogen that can be easily dissociated and used in fuel cells and power plants is not novel, but it has been ongoing for over 40 years (T-Raissi 2002). Recently, the concept of ammonia economy has gained eminence. In the early 1970s when the concept of “Hydrogen Energy Economy” was being widely debated, it was envisioned that ammonia (NH<sub>3</sub>) would provide a perfect storage medium for hydrogen production.

As hydrogen, ammonia is carbon-free and can be produced from any energy resource. However, there are also some significant advantages in terms of storage and transport. Ammonia can be liquefied at room temperature and pressures of 8–10 bar, furthermore, it can be stored in a similar manner to propane, whereas hydrogen requires expensive cryogenic storage mechanisms (Cheddie 2012). Table 2.19 presents the basic physical properties of ammonia.

### **2.9.2.2 Hydrogen Generation from Ammonia**

Hydrogen can be produced from ammonia using different methods. Most of the reported experiences are based on thermal decomposition or catalytically cracking of ammonia into nitrogen and hydrogen. Some papers also address the hydrolysis of ammonia products, as ammonia borane for such a purpose.

#### **Catalytic Decomposition of Ammonia**

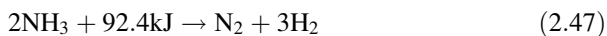


**Table 2.19** Physical properties of ammonia (Adapted from Thomas and Parks 2006)

<i>Hydrogen content</i>					
Hydrogen weight fraction	17.65	wt. %	Hydrogen volume density	0.105	kg/l
<i>Solid phase</i>					
Melting point	−78	°C	Latent heat of fusion (1 atm at triple point)	−337.37	kJ/kg
<i>Liquid phase</i>					
Vapor pressure (21 °C)	8.88	bar	Liquid density (1 atm at boiling point)	682	kg/m <sup>3</sup>
Boiling point (at 1 atm)	−33.5	°C	Liquid/gas equivalent (1 atm and 15 °C)	947	vol/vol
Latent heat of vaporization (1 atm at boiling point)	1371.	kJ/kg			
Critical temperature	132.4	°C	Critical pressure	112.8	bar
<i>Gas phase</i>					
Gas density (1 atm at boiling point)	0.86	3	Gas density 15 °C, 1 atm	0.73	kg/m <sup>3</sup>
Compressibility (Z) (1 atm at 15 °C)	0.9929	Specific gravity (air = 1) (1 atm at 20 °C)	0.597		
Specific volume 1 atm at 20 °C)	1.411	3	Viscosity	.000098	Poise
Heat capacity at constant pressure (Cp) (1 atm at 15 °C)	.037	kJ/(mol K)	Heat capacity at constant volume (Cv) (1 atm at 15 °C)	.028	kJ/(mol K)
Critical density:	0.24	g/mL	Entropy, gas at 25 °C, 1 atm.	45.97	cal/mol °C
Thermal conductivity	22.19	mW/(m K)			
<i>Miscellaneous</i>					
Water solubility (1 atm at 0 °C)	862	vol/vol	Auto ignition temperature	630	°C
Lower flammable limit in air	15 %	By volume	Upper flammable limit in air	28 %	By volume
Molecular weight:	17.03				

Ammonia is unstable at high temperatures and starts decomposing at 200 °C (Cheddar 2012). The slightly endothermic decomposition reaction is shown in Eq. (2.47). Thermodynamically, 98–99 % conversion of ammonia to hydrogen is possible at temperatures that are as low as 425 °C. However, in practice, the conversion rate depends on temperature and catalysts being used. Thermal decomposition or catalytic cracking is the most common method of hydrogen generation from ammonia. For large scale hydrogen generation (>1000 m<sup>3</sup>/h), natural gas reforming remains the most cost-effective process, despite the fact that, on a small-scale generation, (<10 m<sup>3</sup>/h), ammonia cracking becomes slightly less costly than

**Table 2.20** Life cycle cost analysis of hydrogen production via various processes (Lipman and Shah 2007a, b)

Scale of H <sub>2</sub> production (m <sup>3</sup> /h)	Cost of H <sub>2</sub> production, US\$/(m <sup>3</sup> /h)			
	Water electrolysis	Natural gas reforming	Methanol reforming	Ammonia cracking
10	0.943	0.390	0.380	0.343
100	0.814	0.261	0.285	0.279
1000	0.739	0.186	0.226	0.241

natural gas reforming (see Table 2.20) (Lipman and Shah 2007a, b). This result is based on the lifecycle cost analysis, taking into account investment and operation costs.

Early studies conducted on ammonia decomposition are more heavily focused on ammonia synthesis and the so-called iron-based catalysts. Since then, various metals, alloys, and noble metal compounds have been tested for ammonia decomposition. These include Fe, Ni, Pt, Ru, Ir, Pd, Rh; alloys such as Ni/Pt, Ni/Ru, Pd/Pt/Ru/La; and alloys of Fe with other metal oxides, including Ce, Al, Si, Sr, and Zr (Thomas and Parks 2006). Various catalysts have been investigated for decomposing ammonia to produce hydrogen for alkaline fuel cells. These include WC, Ni/Al<sub>2</sub>O<sub>3</sub>, NiCeO<sub>2</sub>/Al<sub>2</sub>O<sub>3</sub>, Cr<sub>2</sub>O<sub>3</sub>, Ru/ZrO<sub>2</sub>, and Ru on carbon nanofibers. Cesium-promoted ruthenium supported on graphite was also found to be very promising (Cairns and Simons. 1968). For these catalysts, a minimum temperature of 300 °C is required for an efficient release of ammonia for hydrogen production.

The catalysts performance can be quantified by using the hydrogen production rate, conversion fraction of ammonia (fraction of ammonia that is converted to hydrogen), and activation energy. The hydrogen generation rate from ammonia decomposition was measured experimentally, typically in units of millimoles of hydrogen produced every minute per gram of catalyst being loaded (mmol/min/g). The performance of various catalysts for ammonia decomposition, reviewed in this section, is summarized in Table 2.21.

Table 2.21 shows that the best ammonia conversion and hydrogen generation rates via thermal decomposition are obtained using Ru/CNT catalysts treated with potassium-based alkalis.

Ni achieves very good results as well, but it requires higher temperatures (500–600 °C) to achieve performance which is equivalent to Ru at 400 °C. The advantage of Ni is that it is less expensive than Ru, and it can be loaded at high concentrations to obtain the desired results.

An anode supported SOFC (with anode thickness of 500 μm, 40 % porosity, and 50 % Ni in volume) requires Ni loading of 0.134 g/cm<sup>2</sup>. If it is operated at a current density of 5000 mA/cm<sup>2</sup>, it consumes hydrogen at 11.6 mmol/min/g of catalyst. If the cell operates at 600 °C, then Ni can safely decompose ammonia at the required rate.

Supports have also been focus of researchers. The support's function is to enhance dispersion, thus increasing the effective area of the active catalyst. The



**Table 2.21** Summary of ammonia decomposition catalysts performance (Lipman and Shah 2007a, b)

Catalyst/support	Temp. (°C)	Rate of H <sub>2</sub> Gen. (mmol/min/g)	Conv. eff. (%)
Nano-sized Ni/Santa Barbara Amorphous (SBA)-15 support	450	8.4	25.0
	500	17.4	52.1
	550	26.8	80.1
	600	31.9	95.2
	650	33.2	99.2
Ni/SBA-15	550	12.7	37.8
Ni/SiO <sub>2</sub>	400	0.4	1.4
	500	3.3	10.5
	550	6.8	21.6
	600	11.4	36.4
	650	21.1	70.0
Ni/SiO <sub>2</sub>	550	11.6	34.6
Ni/Al <sub>2</sub> O <sub>3</sub>	550	12.7	37.8
Ni/Al <sub>2</sub> O <sub>3</sub>	500	24.1	71.9
Ni/Al <sub>2</sub> O <sub>3</sub> coated cordierite monolith	550	16.5	50.0
Ni/Al <sub>2</sub> O <sub>3</sub> (unsupported particles <200 μm)		13.2	40.0
Ir/SiO <sub>2</sub>	400	1.2	3.9
	500	5.7	18.2
	600	17.6	56.0
	700	30.6	98.0
Ru/SiO <sub>2</sub>	400	4.5	14.3
	500	20.0	64
	600	30.3	97
	650	30.9	99
Ru/ZrO <sub>2</sub> Ru/Al <sub>2</sub> O <sub>3</sub>	550	25.8	77.0
		23.5	73.7
Ru/CNT	400	6.2	3.7
Ru/K-CNT		12.2	7.3
Ru/K-ZrO <sub>2</sub> -BD		8.5	5.3
Ru/ZrO <sub>2</sub>		3.7	2.2
Ru/Al <sub>2</sub> O <sub>3</sub>		3.8	2.3
Ru/MgO		5.4	3.2
Ru/TiO <sub>2</sub>		4.3	2.6
Ru/CNT Ru/MgO-CNT		400	6.0
	8.7		13.0
Ru/CNT treated with KNO <sub>3</sub>	400	33.3	49.7
Ru/CNT treated with KOH		31.6	47.2
Ru/CNT treated with K <sub>2</sub> CO <sub>3</sub>		31.3	46.7

All studies were based on an ammonia gas hourly space velocity (GHSV) of 30.000 mL/h/g of catalyst, except for (a) GHSV = 150.000 mL/h/g and (b) GHSV = 60.000 ml/h/g

support should be stable under reaction conditions and have a high specific surface area. For the catalyst Ru, there are various supports, including silica, alumina, graphitized carbon, carbon nanotubes, and nitrogen doped carbon nanotubes (Cheddie 2012). Yin et al. (2004a) ranked the supports for Ru in a decreasing order of activity measured by the ammonia conversion rate: Carbon nanotube (CNT) > MgO > TiO<sub>2</sub> > Al<sub>2</sub>O<sub>3</sub> > ZrO<sub>2</sub> > AC > ZrO<sub>2</sub>/BD. It was proposed that CNTs have had the best performance because they allowed the best dispersion of Ru, and also because of their high purity. CNTs have the additional advantage of presenting high conductivity which aids in electron transfer, thus facilitating the recombinative nitrogen desorption phase. They further showed that the use of the MgO-CNT support resulted in better performance of the catalyst Ru than by using the MgO base or the CNT base alone (Yin et al. 2004b). Temperature-programmed hydrogenation results showed that MgO resulted in an even greater stability for the CNT.

### 2.9.2.3 Production of Hydrogen from Ammonia

A recent comparison of the economics of various methods of hydrogen production showed that the catalytic cracking of ammonia, steam reforming of natural gas and methanol are all more economical methods of hydrogen production than water electrolysis (Silversand 2002). Natural gas reforming is estimated to be the method which involves the lowest cost of production on larger scales, but on small scale production of ten cubic normal meters an hour, ammonia cracking is estimated to be the least costly method. Table 2.22 shows the estimated production costs for these methods as a function of the production rates of ammonia.

In summary, with the anhydrous ammonia, sustainable hydrogen production can be achieved to be used as a fuel source expanding the use of fuel cells in stationary and mobile power generating applications and reducing any inherent emissions of

**Table 2.22** Economic comparison of ammonia cracking and other hydrogen production methods

Unit size (Nm <sup>3</sup> /h)	Electrolysis				Natural gas reforming			
	I	R	M	T	I	R	M	T
10	\$0.286	\$0.64	\$0.014	<b>\$0.943</b>	\$0.286	\$0.09	\$0.014	<b>\$0.390</b>
100	\$0.157	\$0.64	\$0.014	<b>\$0.814</b>	\$0.157	\$0.09	\$0.014	<b>\$0.261</b>
1000	\$0.082	\$0.64	\$0.014	<b>\$0.739</b>	\$0.082	\$0.09	\$0.014	<b>\$0.186</b>
Unit size (Nm <sup>3</sup> /h)	Methanol reforming				Ammonia cracking			
	I	R	M	T	I	R	M	T
10	\$0.214	\$0.15	\$0.014	<b>\$0.380</b>	\$0.143	\$0.19	\$0.014	<b>\$0.343</b>
100	\$0.119	\$0.15	\$0.014	<b>\$0.285</b>	\$0.079	\$0.19	\$0.014	<b>\$0.279</b>
1000	\$0.06	\$0.15	\$0.014	<b>\$0.226</b>	\$0.041	\$0.19	\$0.014	<b>\$0.241</b>

Source: Silversand (2002)

Note: The production costs include investment costs (I), operation costs (R), maintenance costs (M), and total costs (T). All figures were converted to U.S. dollars from the Swedish Krona, using the conversion rate of 6.99 Krona/dollar, and are in units of dollars per cubic normal meter an hour (Nm<sup>3</sup>/h) of hydrogen production

greenhouse gases. Depending on how the ammonia or ammonia complex is initially produced, full fuel-cycle emissions of greenhouse gases and other air pollutants can be moderate or low/zero, which makes a further exploration of these types of systems rather interesting.

## References

- Ahmed A, Abdel M, Farag MAS (2011) Roles of microalgae and bacteria in hydrogen production as one of the renewable energy resources. *Bull Environ Res* 12(2):153–173
- Abreu AJ (2012) Desenvolvimento e caracterização de catalisadores de níquel suportados em matrizes  $\text{CeO-ZrO}_2\text{-Al}_2\text{O}_3$ , 151 f. Teses (Doutorado)—Curso de Curso de Físico-química, Usp, São Carlos
- Aiche T (2005) Steam reforming of methane and bio-ethanol: post-graduate course bioenergy—theory and application. Department of Energy Technology, Fraunhofer Institute for Solar Energy Systems (ISE), Helsinki University of Technology—HUT, pp 18–19
- Aizquierdo U, Barrio VL, Lago N, Requies J, Cambra JF, Guemez MB, Arias PL (2012) Biogas steam and oxidative reforming processes for synthesis gas and hydrogen production in conventional and microreactor reaction systems. *Int J Hydrogen Energy* 37:13829–13842
- Ali T-Raissi (2002) Technoeconomic analysis of area II hydrogen production—Part II. Hydrogen from ammonia and ammonia-borane complex for fuel cell applications. Proceedings of the 2002 U.S. DOE Hydrogen Program Review. NREL/CP-610-32405
- Alves SC (2005) Reforma a Vapor do Metano para a Produção de Hidrogênio: Estudo Termodinâmico e Protótipo de Modelo Matemático de Reator com Membrana. Dissertation, Uberlândia: Universidade Federal de Uberlândia
- Andrade RV (2007) Gaseificação de biomassa: Uma análise teórica e experimental, 205 f. Teses (Doutorado em Engenharia Mecânica)—Instituto de Engenharia Mecânica, Universidade Federal de Itajubá, Itajubá
- ANEEL (Brasil) (2008) Atlas de Energia Eletrica do Brasil: Agencia Nacional de Energia Eletrica, 3rd edn. ANEEL, Brasilia, 236 p
- ANEEL BRASIL (2014) <http://www.aneel.gov.br/aplicacoes/capacidadebrasil/operacaocapacidadebrasil.asp>. Accessed 17 May 2014
- Araki S, Hino N, Mori T, Hikazudani S (2010) Autothermal reforming of biogas over a monolithic catalyst. *J Nat Gas Chem* 19(5):477–481
- Arizona State University. <http://www.asulightworks.com/blog?page=2>. Accessed 17 July 2013
- Avraam DG, Halkides TI, Liguras DK, Bereketidou OA, Goula MA (2010) An experimental and theoretical approach for the biogas steam reforming reaction. *Int J Hydrogen Energy* 35:9818–9827
- Azenha MB (2013) A energia hidrelétrica não é limpa, nem barata. Interview, <http://www.viomundo.com.br/entrevistas/bermann-a-energia-hidreletrica-nao-e-limpa-nem-barata.html>. Accessed 10 Mar 2013
- Basso G, Farret FA, Gonzatti F, Ferrigolo FZ, Franchi D, Miotto M (2013) Projeto e dimensionamento de uma lanta a células a combustível para redução do consumo de energia nos horários de pico de demanda. In: 2º Fórum Internacional Ecoinnovar, Santa Maria, RS
- Basu P (2006) Combustion and gasification in fluidized beds. Taylor & Francis, Abingdon, pp 355–357
- Bertuccioli L, Chan A, Hart D, Lehner F, Madden B, Standen E (2014) Study on development of water electrolysis in the EU. Final report. In: Fuel cells and hydrogen joint undertaking, 160p
- Beurden PV (2004) On the catalytic aspects of steam-methane reforming: a literature survey. ECN-I-04-003

- Bhandari R, Trudewind CA, Zapp P (2014) Life cycle assessment of hydrogen production via electrolysis—a review. *J Cleaner Prod* 85:151–163
- Braga LB (2010) Análise econômica do uso de célula a combustível para acionamento de ônibus urbano, 99 f. Dissertação—Curso de Engenharia Mecânica, Departamento de Energia, UNESP, Guaratinguetá
- Brenna G (2010) New catalyst for the H<sub>2</sub> production by water-gas shift reaction processes. Tese (Doutorado). Curso Química Industrial. Faculdade de Química Industrial. Universidade de Bologna
- Brisse A, Schefold J, Zahid M (2008) High temperature water electrolysis in solid oxide cells. *Int J Hydrogen Energy* 33:5375–5382
- Burgess SJ, Tamburic B, Zemichael F, Hellgardt K, Nixon PJ (2011) Solar driven hydrogen production in green algae. *Adv Appl Microbiol* 75:71–110
- Cai X, Dong X, Lin W (2006) Autothermal REFORMING OF METHANE over Ni catalysts supported on CuO-ZrO<sub>2</sub>-CeO<sub>2</sub>-Al<sub>2</sub>O<sub>3</sub>. *J Nat Gas Chem* 15(2):122–126
- Cairns EJ, Simons EL (1968) Ammonia-oxygen fuel cell. *Nature* 217(5130):780–781
- Casanovas ARM, Leitenburg C, Trovarelli A, Lorca J (2010) Ethanol steam reforming and water gas shift over Co/ZnO catalytic honeycombs doped with Fe, Ni, Cu, Cr and Na. *Int J Hydrogen Energy* 35:7690–7698
- Cheddle D (2012) Ammonia as a hydrogen source for fuel cells: a review. In: Minic D (ed), *Hydrogen energy—challenges and perspectives*. InTech. ISBN: 978-953-51-0812-2
- Chen Y, Wang Y, Xub H, Xiong G (2008) Efficient production of hydrogen from natural gas steam reforming in palladium membrane reactor. *Appl Catal Environ* 80:283–294
- CIRCE (2005) Curso Técnico en Sistemas de Energías Renovables. Centro de Investigación de Recursos y Consumos Energéticos CIRCE, Centro Politécnico Superior, Universidad de Zaragoza, España
- Claassen PAM, de Vrije T (2006) Non-thermal production of pure hydrogen from biomass: HYVOLUTION. *Int J Hydrogen Energy* 31:1416–1423
- Cortés OEJ (2009) Biocombustíveis a partir de microalgas: modelagem e análise de fotobiorreatores. Tese (Doutorado)—Curso Energia e Ambiente, Centro Interdisciplinar de Energia e Ambiente (CIEnAm), Universidade Federal da Bahia
- CRESESB (2012) <http://www.cresesb.cepel.br/sundata/index.php>. Accessed 15 August 2012
- Dantas GA, Leite ALS (2013) Os custos da energia eólica brasileira. [http://www.nuca.ie.ufrj.br/gesel/artigos/05\\_custos\\_energia.pdf](http://www.nuca.ie.ufrj.br/gesel/artigos/05_custos_energia.pdf). Accessed 24 Feb 2013
- Das D, Veziroglu TN (2008) Advances in biological hydrogen production processes. *Int J Hydrogen Energy* 33:6046–6057
- Duane MB, Ariff GD, James BD, Lettow JS, Thomas CE, Kuhn RC (2002) Cost and performance comparison of stationary hydrogen fueling appliances: Task 2 report. In: *Directed Technologies, Inc.* [www.directedtechnologies.com](http://www.directedtechnologies.com)
- Dutra R (2008) CRESESB: Energia Eólica: Princípios e Tecnologia, 58 p
- Effendi A, Hellgardt K, Zhang ZG, Yoshida T (2005) Optimising H<sub>2</sub> production from model biogas via combined steam reforming and CO shift reactions. *Fuel* 84:869–874
- Carnieletto R (2011) Aproveitamento de energia vertida turbinável para produção de hidrogênio e geração distribuída. Universidade Federal de Santa Maria, Santa Maria, p 155
- Energy Options. <http://energy-options.info/2011/03/25/lab-biofuel-now-to-go-into-the-market-place/>. Accessed 17 July 2013
- FAPESP (2013) Revista Pesquisa (Org.). Reforma energética. <http://revistapesquisa2.fapesp.br/?art=3029&bd=1&pg=5&lg>. Accessed 10 Mar 2013
- Foglia D, Wukovits W, Friedl A, Ljunggren M, Zacchi G, Urbaniec K, Markowski M (2011) Effects of feedstock on the process integration of biohydrogen production. *Clean Technol Environ Policies* J 13(4):547–558. doi:10.1007/s10098-011-0351-7
- Furlan AL (2012) Análise técnica e econômica do uso do hidrogênio como meio armazenador de energia elétrica proveniente de fontes eólicas, 86 f. Tese (Doutorado)—Departamento de Engenharia Mecânica, Universidade Estadual de Campinas, Campinas

- Gibson TL, Kelly NA (2009) Predicting efficiency of solar powered hydrogen generation. *Int J Hydrogen Energy* 35:900–911
- Gibson TL, Kelly NA (2008) Optimization of solar powered hydrogen production using photo-voltaic electrolysis devices. *Int J Hydrogen Energy* 33:5931–5940
- Haag S, Burgard M, Ernst B (2007) Beneficial effects of the use of a nickel membrane reactor for the dry reforming of methane: comparison with thermodynamic predictions. *J Catal* 252:190–204
- Hallenbeck PC, Benemann JR (2010) Biohydrogen: the microbiological production of hydrogen fuel. In: Doelle HW, Rokem S (eds) *Biotechnology in EOLSS encyclopedia: biotechnology*, vol 7. ISBN: 978-1-84826-711-4
- Haryanto A, Fernando SD, Filip To SD, Steele PH, Pordesimo L, Adhikari S (2011) High temperature water gas shift reaction over nickel catalysts for hydrogen production: effect of supports, GHSV, metal loading, and dopant materials. *J Thermodyn Catal* 2:106. doi:[10.4172/2153-0645.1000106](https://doi.org/10.4172/2153-0645.1000106)
- Hemschemeier AC (2005) The Anaerobic life of the photosynthetic alga *Chlamydomonas Reinhardtii*. Tese (Doutorado), University of Bochum, Germany
- HY Generation (2014) [http://hy-generation.com/21prod\\_h2.html](http://hy-generation.com/21prod_h2.html). Accessed 10 July 2014
- Inoue T, Kumar SN, Kamachi T, Okura I (1999) Hydrogen evolution from glucose with the combination of Glucose dehydrogenase and Hydrogenase from *A. eutrophus* H16. *Chem Lett* 2:147–148
- IRENA—International Renewable Energy Agency (2013) Summary for policy makers: renewable power generation costs: Abu Dhabi, United Arab Emirates, 12 p
- ITAIPU. <https://www.itaipu.gov.br/energia/energia-disponivel-anual>. Accessed 10 Apr 2014
- Ivy J (2004) Summary of electrolytic hydrogen production, U.S. In: National Renewable Energy Laboratory, Golden, USA
- Koroneos C, Dompros A, Roumbas G, Moussiopoulos N (2004) Life cycle assessment of hydrogen fuel production processes. *Int J Hydrogen Energy* 29:1443–1450
- Kothari R, Buddhi D, Sawhney RL (2008) Comparison of environmental and economic aspects of various hydrogen production methods. *Renew Sustain Energy Rev* 12:553–563
- Krona (2012) <http://www.krona.srv.br/display05.htm>. Accessed 10 Oct 2012
- Kroposki B, Levene J, Harrison K, Sen PK, Novachek F (2006) Electrolysis: information and opportunities for electric power utilities. In: National Renewable Energy Laboratory, NREL/TP-581-40605
- Kuhn J, Kesler O (2015) Carbon deposition thresholds on nickel-based solid oxide fuel cell anodes I. Fuel utilization. *J Power Sources* 277:443–454
- Kwietniewska E, Tys J, Krzeminska I, Kozief W (2012) Microalgae-cultivation and application of biomass as a source of energy: a review. Instytut Agrofizyki im. Bohdana Dobrzańskiego, Lublin
- Larson ED, Williams RH, Regis M, Leal LV (2001) A review of biomass integrated gasifier/gas turbine combined cycle technology and its application in sugarcane industries with an analysis for Cuba. *Energy Sustain Dev* 5(1):54–76
- Lehninger AL, Nelson DL, Cox MM (2010) *Princípios de bioquímica*, 2nd edn. Editora Savier. ISBN 85-7378-026-6
- Levin DB, Pitt L, Love M (2004) Biohydrogen production: prospects and limitations to practical application. *Int J Hydrogen Energy* 29:173–185
- Liguras DK, Kondarides DI, Verykios X (2003) Production of hydrogen for fuel cell by steam reforming of ethanol over supported noble metal catalyst. *Appl Catal B Environ* 43:345–354
- Lipman T, Shah N (2007a). UC Berkeley Transportation Sustainability Research Center, UC Berkeley. <http://www.escholarship.org/uc/item/7z69v4wp>
- Lipman T, Shah N (2007b) Ammonia as an alternative energy storage medium for hydrogen fuel cells. Scientific and Technical Review for Near-Term Stationary Power Demonstration UCB-ITS-TSRC-RR-2007-5
- Logan BE, Hamelers B, Rozendal R, Schröder U, Keller J, Freguia S, Aelterman P, Verstraete W, Rabaey K (2006) Microbial fuel cells: methodology and technology. *Environ Sci Technol* 40:5181–5192. doi:[10.1021/es0605016](https://doi.org/10.1021/es0605016)

- Lopez RA (2004) Célula combustível a hidrogênio: fonte de energia da nova era. Artliber, São Paulo, 182 p
- Ma K, Schicho RN, Kelley RM, Adams MWW (1993) Hydrogenase of the hyperthermophile *Pyrococcus furiosus* is an elemental sulfur reductase or sulfhydrogenase: evidence for a sulfur-reducing hydrogenase ancestor. *Proc Natl Acad Sci USA* 90:5341–5344
- Ma K, Zhou ZH, Adams MWW (1994) Hydrogen production from pyruvate by enzymes purified from the hyperthermophilic archaeon, *Pyrococcus furiosus*: a key role for NADPH. *FEMS Microbiol Lett* 122:245–250
- Maggio G, Freni S, Cavallaro S (1998) Light alcohols/methane fuelled molten carbonate fuel cells: a comparative study. *J Power Sources* 74(1):17–23
- Maia TA, Bellido JDA, Assaf EM, Assaf JM (2007) Produção de hidrogênio a partir da reforma a vapor de etanol utilizando catalisadores Cu/Ni/ $\gamma$ -Al<sub>2</sub>O<sub>3</sub>. *Quim Nova* 30:339–345
- Ministry of Agriculture, Livestock and Food Supply—Secretariat for Production and Agroenergy (2006) Brazilian Agroenergy Plan, Embrapa Publishing House, 118p. [http://www.agricultura.gov.br/pls/portal/docs/page/mapa/planos/pna\\_2006\\_2011/plano%20nacional%20de%20agroenergia%202006%20-%202011-%20ingles.pdf](http://www.agricultura.gov.br/pls/portal/docs/page/mapa/planos/pna_2006_2011/plano%20nacional%20de%20agroenergia%202006%20-%202011-%20ingles.pdf). Accessed 30 Jan 2011
- Paisley MA, Litt RD, Creamer KS (1991) Gasification of refuse-derived fuel in a high throughput gasification system. *Energy Biomass Waste* 14:1991
- Pelczar JRMJ, Chan ECS, Krieg NR (2008) Microbiology, 5th edn. Tata Mc Graw Hill, New York
- Pérez NP, Machin EB, Pedroso DT, Antunes JS, Silveira JL (2014) Fluid-dynamic assessment of sugarcane bagasse to use as feedstock in bubbling fluidized bed gasifiers. *Appl Therm Eng* 73 (1):238–244
- Pimentel TTBC (2012) O Enfrentamento político dos conflitos socioambientais decorrentes da implantação de usinas hidrelétricas. Dissertation, Curso Planejamento de Gestão Ambiental, Universidade Católica de Brasília
- Piroonlerkgul P et al (2008) Selection of appropriate fuel processor for biogas-fuelled SOFC system. *Chem Eng J* 140:341–351
- Raj NT, Goic SR (2011) A review of renewable energy based cogeneration technologies. *Renew Sustain Energy Rev* 15(8):3640–3648
- Reed TB, Das A (1998) Handbook of biomass downdraft gasifier engine systems. The Biomass Energy Foundation Press, Golden
- Roberts JJ (2012) Análise de Desempenho de um sistema Híbrido de Geração de energia solar-eólico-diesel considerando variações probabilísticas da carga e dos recursos renováveis, 151f. Dissertation. Curso Engenharia Mecânica. Faculdade de Engenharia de Guaratinguetá
- Rozendal RA (2007) Hydrogen production through biocatalyzed electrolysis. PhD thesis Wageningen University, Wageningen, The Netherlands
- Saebea D, Arpornwichanop A, Patcharavorachot Y, Assabumrungrat S (2011) Adsorption-membrane hybrid system for ethanol steam reforming: thermodynamic analysis. *Int J Hydrogen Energy* 36:12234–14428
- Sahara Forest Project (2013) <http://www.flickr.com/photos/bellona-foundation/sets/72157626842235875/>. Accessed 18 July 2013
- Sánchez CG, Silva E, Gomes EO (2008) Gaseificação. In: Biomassa para Energia, vol 1, 1 edn. Editora da UNICAMP, Campinas, pp 284–368
- Santos JHT (2004) Avaliação de um sistema de aquecimento do substrato na digestão anaeróbia de dejetos suínos. Dissertation, Universidade Federal de Viçosa
- Scholz M, Melin T, Wessling M (2013) Transforming biogas into biomethane using membrane technology. *Renew Sustain Energy Rev* 17:199–212
- Silva EP (1991) Introdução à tecnologia e economia do hidrogênio. Unicamp, Campinas, p 204. ISBN: 85-268-0174-0
- Silva ME (2005) Análise Termoquímica de Reformador de Etanol: Produção de Hidrogênio para Acionamento de uma Célula a Combustível do Tipo PEM de 1 kW. Guaratinguetá, 108p. Dissertation. Curso em Engenharia Mecânica Departamento de Energia, Faculdade de Engenharia, Campus de Guaratinguetá, Universidade Estadual Paulista

- Silva ME (2010) Análise experimental da reforma a vapor de etanol: aspectos técnicos, econômicos e ecológicos. Tese (Doutorado)—Curso em Engenharia Mecânica. Faculdade de Engenharia de Guaratinguetá, Universidade Estadual Paulista, Guaratinguetá
- Silveira JL (2012) Energia: crise e planejamento. <http://www.comciencia.br/reportagens/energiaeletrica/energia13.htm>. Accessed 2 Mar 2012
- Silveira JL, Braga LB, Souza ACC, Antunes JS, Zanzi R (2009) The benefits of ethanol use for hydrogen production in urban transportation. *Renew Sustain Energy Rev* 13(9):2525–2534
- Silversand F (2002) Catalytic heat exchangers for small-scale production of hydrogen—feasibility study. Svenskt Gastekniskt Center
- Singh RN, Sharma S (2012) Development of suitable photobioreactor for algae production—a review. *Renew Sustain Energy Rev* 16:2347–2353
- Smolinka T, Günther M, Garche J (2011) Status and development potential of water electrolysis for producing hydrogen from renewable sources. National Organisation Hydrogen and Fuel Cell Technology, Berlin
- Sorensen B (2005) Hydrogen and fuel cell: emerging technologies and applications. Elsevier Academic Press, Amsterdam, 450 p
- Souza MMVM (2005) Supported nickel catalysts for steam reforming of methane. In: 2nd Mercosur Congress on Chemical Engineering, 4th Mercosur Congress on Process Systems Engineering, Rio de Janeiro
- Spath PL, Mann (2000) Life cycle assessment of a natural gas combined-cycle power generation system. NREL/TP-570-27715 Colorado: U.S. Department of Energy
- Stein W, Edwards J, Hinkley J, Sattler C (2009) Natural gas: solar-thermal steam reforming. In: *Encyclopedia of electrochemical power sources*, pp 300–312
- Sugai MH (2012) Modelagem matemática de coluna de gaseificação de fotobiorreatores tubulares para cultivo de microalgas. Dissertação em Engenharia Química, Setor de Tecnologia, Universidade Federal do Paraná, Curitiba
- Tamburic B, Zemichael FW, Maitland GC, Hellgardt K (2011) Parameters affecting the growth and hydrogen production of the green algae *Chlamydomonas reinhardtii*. *Int J Hydrogen Energy* 36:7872–7876
- Takeguchi T et al (2002) Study on steam reforming of CH<sub>4</sub> and C<sub>2</sub> hydrocarbons and carbon deposition on Ni-YSZ cermets. *J Power Sources* 112:588–595
- Tao X, Qi F, Yin Y, Dai X (2008) CO<sub>2</sub> reforming of CH<sub>4</sub> by combination of thermal plasma and catalyst. *Int J Hydrogen Energy* 33:1262–1265
- Thomas G, Parks G (2006) Potential roles of ammonia in a hydrogen economy: a study of issues related to the use ammonia for on-board vehicular hydrogen storage. U.S. Department of Energy, February. [http://hydrogen.energy.gov/pdfs/nh3\\_paper.pdf](http://hydrogen.energy.gov/pdfs/nh3_paper.pdf)
- T-Raissi A, Block DL (2004) Hydrogen: automotive fuel of the future. *IEEE Power Energy Mag* 2 (6):40–45
- Trane R, Dahl S, Skjøth-rasmussen MS, Jensen AD (2012) Catalytic steam reforming of bio-oil. *Int J Hydrogen Energy* 37:6447–6472
- University of Nevada (2013) [http://hrc.unlv.edu/renewable/biofuels/rd\\_Photobioreactor.html](http://hrc.unlv.edu/renewable/biofuels/rd_Photobioreactor.html). Accessed 17 July 2013
- Ursúa A, Gandía LM, Sanchis P (2012) Hydrogen production from water electrolysis: current status and future trends. In: *Proceedings of The IEEE 100*, New York, pp 410–426
- Usui N, Ikenouchi M (1997) Biological CO<sub>2</sub> fixation and utilization project by RITE. 1. Highly-effective photobioreactor system. *Energy Convers Manag* 38:487–492
- Van de Beld L (2001) Cleaning of hot producer gas in a catalytic, reverse flow reactor, Final report for: Novem (EWAB Programme, Report No. 9605) and European Commission (AIR Programme, AIR-CT93-1436)
- Van der Meijden CM (2010) Development of the MILENA gasification technology for the production of Bio-SNG. PhD Thesis, ECN-B-10-016
- Vasconcelos N (2006) Reforma a Vapor do Metano em Catalisadores à Base de Níquel Promovidos com Nióbia. Dissertation, Universidade Federal Fluminense, Niterói

- Vreugdenhil BJ, Van der Drift A, Van der Meijden CM (2009) Co-gasification of biomass and lignite in the indirect gasifier Milena. In: Proceeding of Pittsburgh coal conference, Pittsburgh, USA, 20–23 September
- Wang M, Wang Z, Gong X, Guo Z (2014) The intensification technologies to water electrolysis for hydrogen production—a review. *Renew Sustain Energy Rev* 29:573–588
- Wang SJ, Yin SF, Li L, Xu BQ (2004a) Ng CF, Au CT. *Appl Catal B Environ* 52:287
- Wang Y, Chin YH, Rozmiarek RT, Johnson BR, Gao Y, Watson J, Tonkovich AYL, Vander DP (2004b) Highly active and stable Rh/MgO–Al<sub>2</sub>O<sub>3</sub> catalysts for methane steam reforming. *Catal Today* 98:575–581
- Williams RH (1996) Biomass gasifier gas turbine power generating technology. *Biomass Bioenergy* 10(1996):149–166
- Wongchanapai S, Iwai H, Saito M, Yoshida H (2013) Performance evaluation of a direct-biogas solid oxide fuel cell-micro gas turbine (SOFC-MGT) hybrid combined heat and power (CHP) system. *J Power Sources* 223:9–17
- Woodward J, Cordray KA, Edmonston RJ, Blanco-Rivera M, Mattingly SM, Evans BR (2000a) Enzymatic hydrogen production: conversion of renewable resources for energy production. *Energy Fuels* 14:197–201
- Woodward J, Mattingly SM, Danson M, Hough D, Ward N, Adams M (1996) In vitro hydrogen production by glucose dehydrogenase and hydrogenase. *Nat Biotechnol* 14:872–874
- Woodward J, Orr M (1998) Enzymatic conversion of sucrose to hydrogen. *Biotechnol Prog* 14:897–902
- Woodward J, Orr M, Cordray K, Greenbaum E (2000b) Enzymatic production of biohydrogen. *Nature* 405:1014–1015
- Worley M, Yale J (2012) Biomass gasification technology assessment, consolidated report 2012. National Renewable Energy Laboratory (NREL)-SR-5100-57085
- Xu G, Chen X, Honda K, Zhang ZG (2004) Producing H<sub>2</sub>-rich gas from simulated biogas and applying the gas to a 50W PEFC stack. National Institute of Advanced Industrial Science and Technology (AIST). <http://www.interscience.wiley.com>
- Yin SF, Xu BQ, Wang SJ, Ng CF, Au CT (2004a) *Catal Lett* 96:113
- Yin SF, Zhang QH, Xu BQ, Zhu WX, Ng CF, Au CT (2004b) *J Catal* 224:384
- Zainal A (2010) Gasification of lignocellulosic biomass in fluidized beds for renewable energy development. *Renew Sustain Energy Rev* 114:2852–2862



Sustainable Hydrogen Production Processes

Energy, Economic and Ecological Issues

Silveira, J.L. (Ed.)

2017, XIV, 185 p. 92 illus., 72 illus. in color., Hardcover

ISBN: 978-3-319-41614-4